HCS Campaign to Identify Compounds That Inhibit or Disrupt Androgen Receptor-Transcriptional Intermediary Factor 2 Protein-Protein Interactions for the Treatment of Prostate Cancer

Ashley T. Fancher,[1] Yun Hua,[1] Daniel P. Camarco,[1] David A. Close,[1] Christopher J. Strock,[2] and Paul A. Johnston[1,3]

[1]Department of Pharmaceutical Sciences, School of Pharmacy, University of Pittsburgh, Pittsburgh, Pennsylvania.
[2]Apredica, Cyprotex US, Watertown, Massachusetts.
[3]University of Pittsburgh Medical Center, Hillman Cancer Center, Pittsburgh, Pennsylvania.

ABSTRACT

Twenty percent of prostate cancer (PCa) patients develop a noncurable drug-resistant form of the disease termed castration-resistant prostate cancer (CRPC). Overexpression of Androgen Receptor (AR) coactivators such as transcriptional intermediary factor 2 (TIF2) is associated with poor CRPC patient outcomes. We describe the implementation of the AR-TIF2 protein-protein interaction biosensor (PPIB) assay in a high-content screening (HCS) campaign of 143,535 compounds. The assay performed robustly and reproducibly and enabled us to identify compounds that inhibited dihydrotestosterone (DHT)-induced AR-TIF2 protein-protein interaction (PPI) formation or disrupted preexisting AR-TIF2 PPIs. We used multiparameter HCS data z-scores to identify and deprioritize cytotoxic or autofluorescent outliers and confirmed the resulting qualified actives in triplicate. None of the confirmed AR-TIF2 PPIB inhibitors/disruptors exhibited activity in a p53-hDM2 PPIB counter screen, indicating that they were unlikely to be either nonselective PPI inhibitors or to interfere with the biosensor assay format. However, eight confirmed AR-TIF2 PPIB actives also inhibited the glucocorticoid receptor (GR) nuclear translocation counter screen by >50%. These compounds were deprioritized because they either lacked AR specificity/selectivity, or they inhibited a shared component of the AR and GR signaling pathways. Twenty-nine confirmed AR-TIF2 PPIB actives also inhibited the AR nuclear localization counter screen, suggesting that they might indirectly inhibit the AR-TIF2 PPIB assay rather than directly blocking/disrupting PPIs. A total of 62.2% of the confirmed actives inhibited the DHT-induced AR-TIF2 PPI formation in a concentration-dependent manner with $IC_{50}s < 40\,\mu M$, and 59.4% also disrupted preexisting AR-TIF2 PPI complexes. Overall, the hit rate for the AR-TIF2 PPIB HCS campaign was 0.12%, and most hits inhibited AR-TIF2 PPI formation and disrupted preexisting AR-TIF2 complexes with similar AR-red fluorescent protein distribution phenotypes. Further secondary and tertiary hit characterization assays are underway to select AR-TIF2 PPI inhibitor/disruptor hits suitable for medicinal chemistry lead optimization and development into novel PCa/CRPC therapeutics.

Keywords: androgen receptor, transcriptional intermediary factor 2, protein-protein interactions, biosensor, high content imaging

INTRODUCTION

Prostate cancer (PCa) is the second leading type of cancer in men in the United States, behind skin cancer.[1] Twenty percent of PCa patients develop a noncurable form of the disease termed castration-resistant prostate cancer (CRPC). The prognosis for CRPC is terminal, and the mean survival of patients with metastatic CRPC is only 9–13 months.[2] The current standard of care treatment options for patients with PCa are surgery and radiation for a more localized tumor, and androgen deprivation therapy (ADT) for recurrent or metastatic tumors.[3,4] Since CRPC cells continue to rely on androgen receptor (AR) signaling for growth and proliferation, ADT drugs modulate AR functions in a direct manner by antagonizing the receptor itself, or in an indirect manner by blocking androgen synthesis.[5] Although ADTs are effective initially, almost all patients progress to a castrate-resistant state. Even the two most recently FDA-approved drugs for CRPC therapy, the AR

antagonist enzalutamide and androgen synthesis inhibitor abiraterone, provide only a modest 3–5 month survival benefit to patients,[6,7] underscoring the urgent need to identify and develop novel drugs for the treatment of CRPC.

Multiple mechanisms of resistance arise in CRPC cells that render ADT drugs ineffective. Mechanisms of resistance include AR amplification, intratumoral androgen synthesis, AR mutations that lead to receptor promiscuity, the emergence of AR splice variants, and androgen-independent AR activation.[8] Furthermore, most cases of CRPC are accompanied by overexpression of AR coactivators, which lead to poor patient outcomes by increasing AR-transcriptional activity.[9] Ligand-activated AR traffics from the cytoplasm into the nucleus, where it binds to DNA at specific androgen-responsive elements (AREs) on the promoters of AR target genes, recruit coactivators that enable histone remodeling, additional coactivator recruitment, and subsequent assembly of the transcriptional machinery.[10] AR target genes are associated with cellular biosynthesis, survival, and proliferation, leading to disease progression.[11] Therefore, therapeutics that target AR-transcriptional activity represent an alternate strategy for slowing the progression of CRPC. One strategy to target AR's transcriptional activity would be to block the recruitment of the transcriptional machinery to target gene AREs by preventing or disrupting the interactions between AR and its co-activators.[12–20] Elevated expression levels have been observed in relapsed CaP for several AR co-regulators, including TIF2, SRC-1, RAC3, p300, CBP, Tip60, MAGE-11, and ARA 70.[12–15,17,20–23] AR-transcriptional intermediary factor 2 (TIF2/SRC-2/NCoA-2/GRIP1) protein-protein interactions (PPIs) are promising targets for CRPC because TIF2 overexpression occurs in more advanced stages of PCa compared to benign prostate tissue, and increased TIF2 levels correlate with biochemical recurrence, a rise in prostate specific antigen (PSA) levels in PCa patients.[9] Similarly, knockdown of TIF2 by siRNA reduced AR target gene expression and slowed the proliferation of androgen-dependent and androgen-independent PCa cells.[12] The AR interacts with TIF2 through the hydrophobic activation function 2 (AF2) region formed by helix 12 of the androgen receptor ligand binding domain (AR-LBD) when dihydrotestosterone (DHT) is bound.[24] TIF2 modulates AR-transcriptional activity and its overexpression has been shown to result in cellular resistance to AR antagonists such as bicalutamide.[25] We therefore developed a high-content screening (HCS) assay to identify small molecules that inhibit the formation of agonist-induced AR-TIF2 PPIs or disrupt preexisting AR-TIF2 complexes.[26–28]

The AR-TIF2 PPI HCS assay utilizes two adenovirus constructs to express AR-LBD residues 662–919 in one biosensor component, and TIF2 residues 725–840 in the other biosensor component.[26–28] AR-LBD was cloned into an adenovirus expression biosensor construct that drives its expression as a chimeric fusion protein with red fluorescent protein (RFP) that contains both nuclear localization sequence (NLS) and nuclear export sequence (NES), which are part of the chimera and not specific to AR. The TIF2 insert contains the receptor-interacting domain box III LXXLL motif that mediates binding to ligand-bound AR-LBD, and the TIF2 residues are expressed as a chimeric fusion protein with green fluorescent protein (GFP) and a high-affinity NLS/nucleolar localization sequence (NoLS) derived from HIV Rev, which tethers the TIF2-GFP biosensor in the nucleolus of the cell. The development, optimization, and validation of the AR-TIF2 protein-protein interaction biosensor (PPIB) HCS assay, together with suitable counter screens and secondary assays, have been described previously.[26–34] In addition to AR-TIF2 PPI inhibitors and disruptors, AR antagonists and heat shock protein (HSP) 90 inhibitors can also block DHT-induced AR-TIF2 PPI formation.[26–28] Herein, we report the use of the AR-TIF2 PPI HCS assay to conduct an HCS campaign of 143,535 compounds from three compound libraries: a 10,000-compound ChemDiv PPI library, a 50,000-compound ChemBridge diversity library, and an 83,535-compound library, provided by the NCI's Chemical Biology Consortium (CBC) small molecule repository. The AR-TIF2 PPIB assay was screened in two formats, to determine if compounds could block DHT-induced AR-TIF2 PPI formation, and to identify compounds that could disrupt preexisting AR-TIF2 PPI complexes. The results of the primary AR-TIF2 PPI HCS, cytotoxic and fluorescent outlier triage, active confirmation, counter screens, and IC_{50} determinations of the hits are presented below.

METHODS AND MATERIALS

Reagents

Nutlin-3, formaldehyde, DHT, dexamethasone (Dex), tetracycline (Tet), and 17-allylaminogeldanamycin (17-AAG) were all purchased from Sigma-Aldrich (St. Louis, MO). Dimethyl sulfoxide (DMSO) (99.9% high-performance liquid chromatography grade, under argon) was purchased from Alfa Aesar (Ward Hill, MA). Dulbecco's Mg^{2+}- and Ca^{2+}-free phosphate-buffered saline (PBS) was purchased from Corning (Tewksbury, MA). Hoechst 33342 was purchased from Invitrogen (Carlsbad, CA).

Cells and Tissue Culture

The U-2 OS osteosarcoma cell line was acquired from American Type Culture Collection and was maintained in McCoy's 5A medium with 2 mM L-glutamine (Invitrogen)

supplemented with 10% fetal bovine serum (FBS) (Gemini Bio-Products, West Sacramento, CA), and 100 U/mL penicillin and streptomycin (Invitrogen) in a humidified incubator at 37°C, 5% CO_2, and 95% humidity. The N3 C4-2-2GFP-AR stable cell line expressing 2GFP-AR was kindly provided by Dr. Zhou Wang in the Urology department of the University of Pittsburgh Hillman Cancer Institute and was maintained in RPMI-1640 medium supplemented with 10% FBS, 1% L-glutamine, 100 U/mL penicillin and streptomycin, and 800–1,000 μg/mL G418 (Gemini Bio-Products) in a humidified incubator at 37°C, 5% CO_2, and 95% humidity.[33] The 3617.4 mouse mammary adenocarcinoma cell line stably expressing a rat glucocorticoid nuclear hormone receptor green fluorescent fusion protein (glucocorticoid receptor-GFP [GR-GFP]) under the control of a Tet-regulated promoter was kindly provided by Dr. Gordon Hager (Laboratory of Receptor Biology and Gene Expression; NCI, Bethesda, MD).[35–37] The 3617.4 cell line was maintained in a complete culture medium containing 10 μg/mL tetracycline (Tet-on) in a humidified incubator at 37°C, 5% CO_2, and 95% humidity to keep the expression of GR-GFP repressed: Dulbecco's modified Eagle's medium (DMEM) with 2 mM L-glutamine (Invitrogen) supplemented with 10% FBS (Gemini Bio-Products), 100 μM nonessential amino acids (Invitrogen), 100 μM sodium pyruvate (Invitrogen), and 100 U/mL penicillin and streptomycin (Invitrogen), and containing 0.96 mg/mL G418 (Invitrogen).[29,34]

Compound Libraries and Compound Handling

We screened three compound libraries totaling 143,535 compounds in the AR-TIF2 PPIB HCS campaign: a 10,000-compound library purchased from ChemDiv (San Diego, CA), a 50,000-compound library that was purchased from ChemBridge (San Diego, CA), and an 83,535-compound library provided by the NCI's CBC small molecule repository. The 10K ChemDiv nonpeptide peptido-mimetic compound lîbrary represents a diversity subset of their 142,000-compound PPI library that includes mimetics of α-helices and β/γ-turns based on several combinatorial templates modified with both flexible and rigid substituents. The geometry of the designed fragments was compared computationally with the dihedral angles reported for "natural" β- and γ-turn motifs to select the best matched compounds. Dipeptide and tripeptide mimetics together with RGD, AVPI, PDZ, and VIP domain binding motifs are also included. The 10K ChemDiv PPI diversity library was supplied in a 96-tube array at a concentration of 5 mg/mL in DMSO that we reformatted by quad-mapping onto 384-well plates. The ChemDiv PPI diversity library was screened in the primary AR-TIF2 PPIB HCS assay at 10 μg/mL and 0.2% DMSO. The ChemBridge 50,000-compound diversity library was selected from a 410,000-compound core library and was designed to provide the widest coverage of pharmacophore space within 50,000 compounds, while maintaining structural diversity. Compounds were filtered for enhanced physiochemical properties, while allowing exploration of available chemical space: MW ≤500, clogP ≤5, tPSA ≤100, rotatable bonds ≤8, hydrogen bond acceptors ≤10, and hydrogen bond donors ≤5. Nondrug-like compounds and undesirable chemical groups (*e.g.*, Michael acceptors, crown-ethers and analogs, disulfides, and epoxides) were removed, as were structural, salt, and tautomeric duplicates. A 3D conformational analysis was used to identify all 3-point pharmacophores within the subset of filtered compounds and a structural diversity measure was applied to select a set of 50,000 compounds. The ChemBridge diversity library was supplied arrayed in 384-well plates at a concentration of 10 mM in DMSO and was screened in the primary AR-TIF2 PPIB HCS assay at 25 μM and 0.25% DMSO. RO1 funding support from the NCI qualified us to obtain a copy of the NCI's CBC NExT program compound library. The 83,535-compund NCI CBC library was specifically assembled for anti-cancer drug screening and contains a 12,000-compound legacy set selected from the NIH Molecular Library Small Molecule Repository (MLSMR) collection, and two diversity subsets that contain 15 privileged scaffolds. The 83K NCI CBC library was arrayed in 384-well plates at a concentration of 10 mM in DMSO and was screened in the primary AR-TIF2 PPIB HCS assay at 20 μM and 0.2% DMSO. Replica daughter plate sets were prepared, stored at −20°C, and handled as described previously.[27,34,38–41]

To determine 50% inhibition concentrations (IC_{50}), 10-point twofold or threefold serial dilutions of test compounds in 100% DMSO were performed using a 384-well P30 dispensing head on the Janus MDT automated liquid handling platform (Perkin Elmer, Waltham, MA), as described previously.[27,34,38–41] Daughter plates containing 2 μL of the serially diluted compounds in DMSO were prepared and replicated from the 384-well serial dilution master plates using the Janus MDT platform outfitted with a 384-well transfer head. Aluminum adhesive plate seals were applied, and plates were stored at −20°C. For testing in bioassays, daughter plates were withdrawn from −20°C storage, thawed to ambient temperature, centrifuged 1 min at 100 × *g*, and the plate seals were removed before the transfer of 38 μL of serum-free media into wells using the BioTek Microflo liquid handler (BioTek, Winooski, VT) to generate an intermediate stock concentration of library compounds ranging from 1.95 to 500 μM (5.0% DMSO). The diluted compounds were mixed by repeated aspiration and dispensation using a 384-well P30 dispensing head on the

Janus MDT platform and then 5 μL of diluted compounds was transferred to the wells of assay plates to provide a final concentration response ranging from 0.195 to 50 μM (0.5% DMSO).

AR-TIF2 PPIB Primary HCS Assay

The automated AR-TIF2 PPIB HCS assay performed in either U-2 OS or PC-3 PCa cells was described previously.[26–28] Briefly, recombinant adenovirus expression constructs (Cyprotech US, Watertown, MA) bearing the individual TIF2-GFP (Tag GFP; Evrogen, Inc., Moscow, Russia) and AR-RFP (Tag RFP; Evrogen, Inc.) PPI partners were used to co-infect U-2 OS cells. Typically, U-2 OS cells co-infected with the TIF2-GFP and AR-RFP adenovirus constructs were seeded at 2,500 cells per well in 384-well collagen-coated barcoded microplates (No. 781956; Greiner BioOne) using a BioTek Microflo liquid handler (BioTek), and plates were incubated overnight at 37°C in 5% CO_2 and 95% humidity. To determine if compounds could block DHT-induced AR-TIF2 PPI formation, assay plates were preincubated with compounds at 37°C in 5% CO_2 and 95% humidity for 3 h before the addition of 25 nM DHT for 90 min. To investigate whether compounds could disrupt preexisting AR-TIF2 PPI complexes, assay plates were preincubated with 25 nM DHT for 90 min before the transfer of compounds and an additional 3-h incubation at 37°C in 5% CO_2 and 95% humidity. Maximum plate control wells ($n = 32$) in columns 1 and 2 were exposed to 25 nM DHT and ≤0.25% DMSO, and minimum plate control wells ($n = 32$) in columns 23 and 24 were treated with ≤0.25% DMSO. Diluted compounds or DMSO (5 μL) were transferred to wells using a Janus MDT automated liquid handling platform (Perkin-Elmer, Waltham, MA) outfitted with a 384-well transfer head. DHT (5 μL, maximum plate controls and compound-treated wells) or media (5 μL, minimum plate controls) were added to the appropriate wells to achieve a final DHT concentration of 25 nM. After the appropriate DHT and compound exposure periods, assay plates were fixed by the addition of 50 μL of prewarmed (37°C) 7.4% formaldehyde and 2 μg/mL Hoechst 33342 in PBS using a BioTek ELx405 (BioTek) and incubated at room temperature for 30 min. Liquid was then aspirated, and plates were then washed twice with 85 μL PBS using a BioTek ELx405 plate washer, leaving the final wash in the plate. The plates were then sealed with adhesive aluminum plate seals. Fluorescent images of three fields of view in each of the DAPI (Hoechst-stained nuclei), FITC (TIF2-GFP), and Texas Red (AR-RFP) channels were acquired on an ImageXpress Micro (IXM) automated HCS platform (Molecular Devices LLC, Sunnyvale, CA) using a 10×Plan Fluor 0.3 NA objective. Images were then analyzed using the translocation-enhanced (TE) image analysis module of the MetaXpress software (Molecular Devices LLC) as described previously.[26–28]

p53-hDM2 PPIB Counter Screening Assay

The p53-hDM2 PPIB HCS assay performed in U-2 OS cells has also been described previously.[30–32] Briefly, recombinant adenovirus expression constructs (Cyprotech US) bearing the individual p53-GFP (Tag GFP; Evrogen, Inc.) and hDM2-RFP (Tag RFP; Evrogen, Inc.) PPI partners were used to co-infect U-2 OS cells, and cells were seeded at 2,500 cells per well in 384-well collagen-coated barcoded microplates (No. 781956; Greiner BioOne) using a BioTek Microflo liquid handler, and plates were incubated overnight at 37°C in 5% CO_2 and 95% humidity. To determine if compounds could disrupt p53-hDM2 PPI complexes, assay plates were exposed to compounds for 3 h at 37°C in 5% CO_2 and 95% humidity. Maximum plate control wells ($n = 32$) in columns 1 and 2 were exposed to 10 μM Nutlin-3 and ≤0.25% DMSO, and minimum plate control wells ($n = 32$) in columns 23 and 24 were treated with ≤0.25% DMSO. Compounds or plate controls (5 μL) were added to appropriate wells using a Janus MDT liquid handling platform (Perkin-Elmer) outfitted with a 384-well transfer head and plates were incubated at 37°C for 3 h. After the appropriate Nutlin-3 and compound exposure periods, assay plates were fixed by the addition of 50 μL of prewarmed (37°C) 7.4% formaldehyde and 2 μg/mL Hoechst 33342 in PBS using a BioTek ELx405 (BioTek) and incubated at room temperature for 30 min. Liquid was then aspirated, and plates were then washed twice with 85 μL PBS using a BioTek ELx405 plate washer, leaving the final wash in the plate. The plates were then sealed with adhesive aluminum plate seals. Fluorescent images of two fields of view in each of the DAPI (Hoechst-stained nuclei), FITC (p53-GFP), and Texas Red (hDM2-RFP) channels were acquired on an IXM automated HCS platform using a 10×Plan Fluor 0.3 NA objective. Images were then analyzed using the TE image analysis module of the MetaXpress software consistent with the ArrayScan V^{Ti} molecular translocation algorithm described previously.[30–32]

AR Nuclear Localization Counter Screen

The AR nuclear localization HCS assay was performed as described previously.[33] Briefly, N3 C4-2-2GFP-AR cells were seeded into 384-well, black-walled clear-bottom plates (Cat No. 781091; Greiner Bio-one) at a density of 3,000 cells/well in complete media and cultured overnight. The cells were then treated overnight with DMSO vehicle, DMSO in the presence of the compounds in the library, or DMSO plus 3.0 μM 17-AAG. Maximum plate control wells ($n = 32$) in columns 1 and 2 were exposed to ≤0.25% DMSO, and minimum plate control wells ($n = 32$) in columns 23 and 24 were treated with 3.0 μM 17-AAG plus ≤0.25% DMSO. The treated cells were subsequently fixed using prewarmed (37°C) 3.7% formaldehyde

containing 2 μg/mL Hoechest 33342 in PBS at room temperature for 30 min. Liquid was then aspirated, and plates were then washed twice with 50 μL PBS using a BioTek ELx405 plate washer and sealed with adhesive aluminum plate seals with the last 50 μL wash of PBS in place. Fluorescent images of two fields of view in each of the DAPI (Hoechst-stained nuclei) and FITC (2GFP-AR) channels were sequentially acquired on the IXM HCS platform using a 10× Plan Fluor 0.3 NA objective. Images were then analyzed using the TE image analysis module of the MetaXpress software consistent with the ArrayScan V^{Ti} Molecular Translocation algorithm described previously.[33]

Dex-Induced GR Translocation Counter Screen

The Dex-induced GR-GFP nuclear translocation HCS assay was performed as described previously.[29,34] To induce GR-GFP expression in the 3617.4 cell line, cells were cultured in a Tet-free induction medium (Tet-off) in a humidified incubator at 37°C, 5% CO_2, and 95% humidity: DMEM with 2 mM L-glutamine (Invitrogen) supplemented with charcoal-stripped 10% FBS (Gemini Bio-Products), 100 μM nonessential amino acids, 100 μM sodium pyruvate, and 100 U/mL penicillin and streptomycin, and containing 0.96 mg/mL G418.[29,34] In the Tet-free induction medium, 3617.4 cells were seeded at 2,500 cells per well in 384-well, black-walled clear-bottom plates (Cat No. 781091; Greiner Bio-One) in a volume of 60 μL using the Microflo liquid handler (BioTek). Plates were incubated under Tet-off conditions for 48 h at 37°C and 5% CO_2 in a humidified incubator and then, diluted compounds (20 μL) were added to wells in columns 3 through 22 using a Janus MDT liquid handler (Perkin-Elmer) outfitted with a 384-well transfer head. Compound-treated plates were incubated at 37°C and 5% CO_2 in a humidified incubator for 60 min and then, 20 μL of 5.0 μM Dex (1.0 μM final in well) was transferred to assay plates using the Janus MDT liquid handler outfitted with a 384-well transfer head. Maximum plate control wells ($n=32$) in columns 1 and 2 were exposed to 1.0 μM Dex and ≤0.25% DMSO, and minimum control wells ($n=32$) in columns 23 and 24 were treated with ≤0.25% DMSO. Assay plates were incubated for 30 min at 37°C in 5% CO_2 and 95% humidity and then, the contents of the wells were aspirated and replaced with 50 μL of 3.7% formaldehyde containing 2 μg/mL Hoechst 33342 in PBS without Ca^{2+} and Mg^{2+}, prewarmed to 37°C, using a BioTek ELx405 (BioTek) plate washer, and cells were fixed for 10–30 min at ambient temperature. The fixative was then aspirated, and plates were then washed twice with 50 μL PBS using the BioTek ELx405 plate washer and sealed with adhesive aluminum plate seals with the last 50 μL PBS wash in place. Fluorescent images of two fields of view in each of the DAPI (Hoechst-stained nuclei) and FITC (GR-GFP) channels were then acquired on the IXM automated imaging platform using a 10× Plan Fluor 0.3 NA objective. Images were then analyzed using the TE image analysis module consistent with the ArrayScan V^{Ti} Molecular Translocation algorithm described previously.[29,34]

Image Acquisition on the IXM Automated Imaging Platform

The IXM is an automated wide-field high-content imaging platform integrated with the MetaXpress Imaging and Analysis software (Molecular Devices LLC). The IXM optical drive includes a 300 W Xenon lamp broad-spectrum white light source and 2/3″ chip cooled CCD camera and optical train for standard field of view imaging with transmitted light and phase contrast options. The IXM is equipped with a 4× Plan Apo 0.20 NA objective, a 10× Plan Fluor 0.3 NA objective, a 20× Ph1 Plan Fluor ELWD DM objective, a 20×, S Plan Fluor ELWD 0.45 NA objective, and a 40×, S Plan Fluor ELWD 0.60 NA objective. The IXM is equipped with the following Zero Pixel Shift filter sets; DAPI, FITC/ALEXA 488, CY3, CY5, and Texas Red.

Image Analysis Using the TE Module

We utilized the TE image analysis module to analyze and quantify AR-TIF2 and p53-hDM2 PPIs from digital images acquired on the IXM as described previously.[26–28,30–32] For the AR-TIF2 PPIB assay, we used the TIF2-GFP biosensor component in the FITC channel to create a translocation mask of the nucleoli within Hoechst-stained nuclei. The TIF2-GFP remains localized to bright fluorescent puncta anchored within the nucleolus, and objects in Ch2 that had TIF2-GFP fluorescent intensities above background with appropriate morphologic characteristics (width, length, and area) were classified by the image segmentation as nucleoli and used to create a TIF2 mask and count the number of TIF2-GFP-positive nucleoli. Objects that met these criteria were used to create masks of the nucleoli within the Hoechst-stained nuclei of each cell. AR-RFP images from the Texas Red channel were segmented into an "Inner" nucleolus region with a mask set using the edge of the detected TIF2-GFP-positive nucleoli in the FITC channel. The TE image analysis module outputs quantitative data such as the average fluorescence intensities of the TIF2-GFP-stained objects in the FITC channel; the selected object or nucleoli count in the FITC channel; and the integrated and average fluorescent intensities of the AR-RFP signal in the TIF2-positive nucleolus (inner) region. The mean average inner fluorescent intensity (MAIFI) of AR-RFP within the TIF2-GFP-positive nucleolus output of the TE image analysis module was used to quantify AR-TIF2 PPIs.[26–28] For the p53-hDMs PPIB counter screening assay, we used the same TE image analysis strategy, except that it is the

p53-GFP biosensor that is anchored within the nucleolus of Hoechst-stained nuclei that are used to create a p53 mask and count the number of p53-GFP-positive nucleoli. hDM2-RFP images from the Texas Red channel were then segmented into an "Inner" nucleolus region with a mask set using the edge of the detected p53-GFP-positive nucleoli in the FITC channel. The MAIFI of hDM2-RFP within the p53-GFP-positive nucleolus output of the TE image analysis module was used to quantify p53-hDM2 PPIs.[30–32]

To analyze the digital images from the Dex-induced GR-GFP nuclear translocation and AR-GFP nuclear localization assays, we used a TE image analysis module that is analogous to the ArrayScan V^{Ti} Molecular Translocation algorithms described previously.[29,33,34] Hoechst DNA-stained objects in the DAPI channel that exhibited fluorescent intensities above a background threshold and had suitable morphology (width, length, and area) characteristics were classified by the TE image segmentation as nuclei and were used to create nuclear masks for each cell. The nuclear mask was then eroded 1 μm in from the edge of the detected nucleus and a reduced "inner" mask was established to quantify the target GR-GFP or AR-GFP fluorescence within the nucleus. An FITC channel "outer" cytoplasm mask was then established 1 μm out from the edge of the detected nucleus and the width was set at 3 μm, to cover a region of the cytoplasm within the cell boundary. The FITC channel "outer" mask was used to quantify the amount of target GR-GFP or AR-GFP fluorescence within this region of the cytoplasm. The TE image analysis module outputs quantitative individual cell or well-averaged data, including the selected object or cell counts per image in the DAPI channel, together with the average or integrated fluorescent intensities of the GR-GFP or AR-GFP FITC channel signals in the "inner" nuclear and "outer" cytoplasmic regions of the cell. The MAIFI of GR-GFP or AR-GFP output of the TE image analysis module was used to quantify Dex-induced GR-GFP nuclear translocation and AR-GFP nuclear localization, respectively.[29,33,34]

Cytotoxic and Fluorescent Outlier Analysis

We employed a z-score plate-based statistical scoring method to flag compounds that behaved as outliers compared to the other substances ($n = 320$, no controls) tested on an assay plate for selected HCS multiparameter measurement output by the image analysis module, $Z - score = (X_i - \overline{X})/\sigma$, [31,33,42] where X_i is the raw measurement on the ith compound, and $\overline{X}$ and σ are the mean and standard deviation of all the sample measurements on a plate. We utilized the number of compartments that represents the number of TIF2-GF-positive nucleoli identified in the FITC channel to flag compounds that were cytotoxic, and compounds with z-scores <–3 were flagged as cytotoxic. We calculated z-scores for the average and integrated fluorescent intensity parameters from the DAPI, FITC, and Texas Red channels, and compounds with z-scores >3 in one or more of the intensity parameters in any channel were flagged as fluorescent outliers.

Data Processing, Visualization, Statistical Analysis, and IC_{50} Curve Fitting

An HTS template was utilized to normalize bioassay data as % inhibition based on the performance of assay plate controls and to calculate signal-to-background (S:B) ratios and Z'-factor coefficient assay performance quality control (QC) statistics. In each of the 384-well HCS assays, minimum ($n = 32$) and maximum ($n = 32$) plate control wells were utilized to normalize the signals in the compound-treated wells and to represent 0% and 100%, respectively. IC_{50} values for each of the bioassays were calculated using GraphPad Prism 5 software to plot and fit data to curves using the sigmoidal dose–response variable slope equation $Y = \text{Bottom} + [\text{Top} - \text{Bottom}]/[1 + 10^{(\text{LogEC50}-X)} \times \text{Hill Slope}]$.

RESULTS

AR-TIF2 PPIB Assay Principle and HCS Performance

The AR-TIF2 biosensor assay was performed in U-2 OS cells co-infected with two recombinant adenoviruses to express the AR and TIF2 PPIB partners in cells (*Fig. 1*).[26–28] We used U-2 OS cells for the HCS for logistical reasons because, although the AR-TIF2 PPIB assay can be performed in PC-3 cells, they require ~10-fold more rAV for infection and a twofold to fourfold higher cell seeding density than U-2 OS cells.[26] The AR-RFP "prey" protein interaction partner shuttles between the cytoplasm and nucleus in a ligand-dependent manner and is composed of AR residues 662–919 encoding the AR-LBD and AF2 surface as a chimeric fusion protein with RFP and both NLS and NES. The TIF2-GFP "bait" protein interaction partner is targeted to and anchored in the nucleoli within the cell nucleus, and expresses TIF2 residues 725–840 containing a box III α-helical LXXLL motif to mediate the binding to ligand-bound AR as a chimeric fusion protein with GFP and a high-affinity NLS/NoLS derived from HIV Rev.[26–28] Representative images of the AR-TIF2 PPI assay plate controls are presented in *Figure 1B*. In DMSO-treated U-2 OS cells co-infected with both biosensors, AR-RFP expression is localized predominantly to the cytoplasm and TIF2-GFP expression is localized only to nucleoli, as indicated in the cartoon and color composite images of cells with a diffuse red cytoplasm and blue Hoechst-stained nuclei containing bright green TIF2-GFP puncta (*Fig. 1A, B*). After exposure to the AR agonist DHT, the AR-RFP biosensor traffics into the nucleus and co-localizes with the TIF2-GFP biosensor

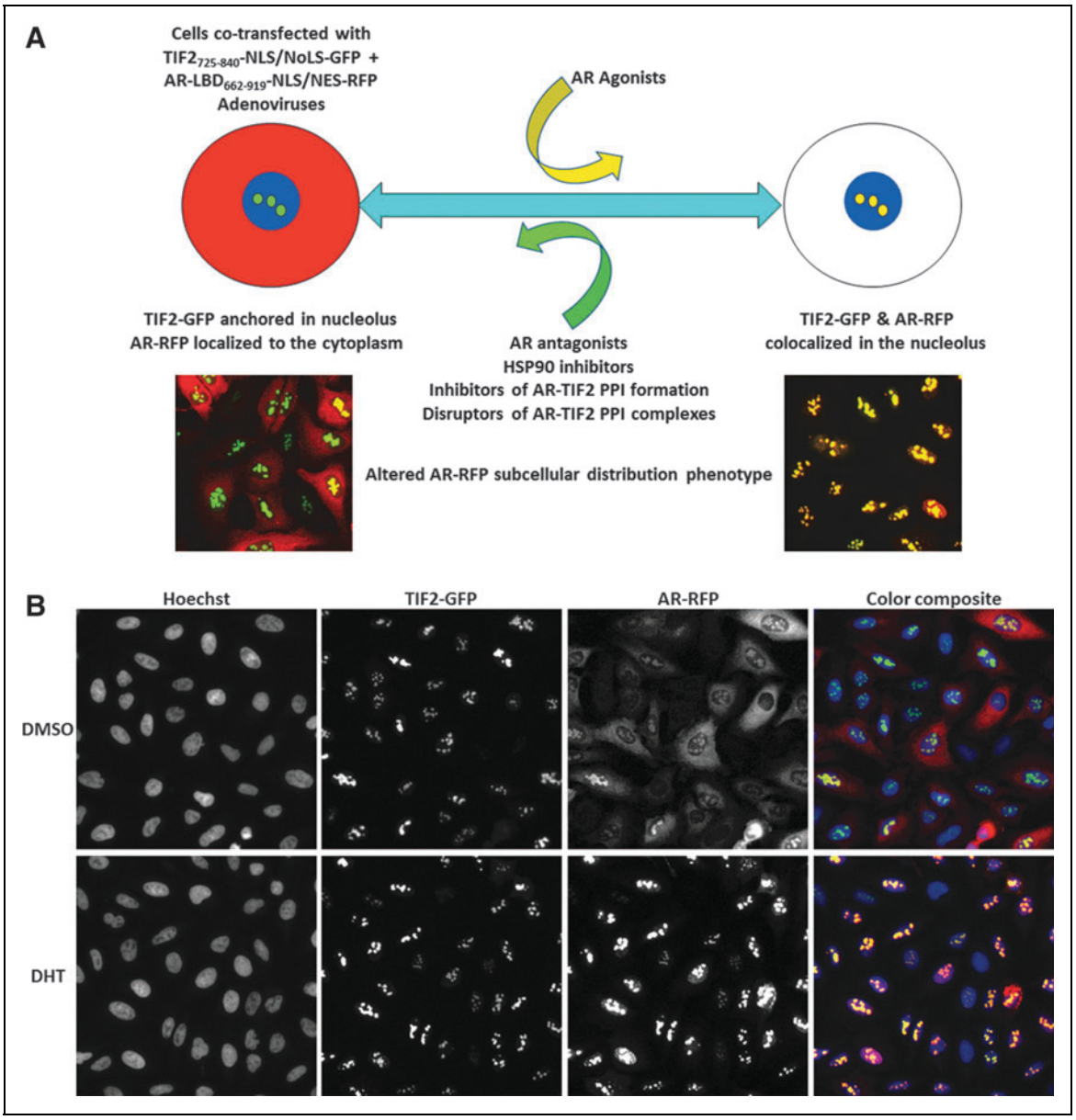

Fig. 1. AR-transcription intermediary factor 2 PPI HCS assay; **(A)** assay principle, **(B)** representative images of assay plate controls. **(A)** The AR-TIF2 biosensor assay recapitulates the ligand-induced translocation of AR from the cytoplasm to the nucleus, and the PPIs between AR and TIF2 result in the co-localization of AR-RFP and TIF2-GFP within the nucleolus. The DHT-induced change in the AR-RFP subcellular distribution phenotype from a predominantly cytoplasmic distribution in untreated cells to a punctate distribution co-localized with TIF2-GFP in the nucleoli of the nuclei in treated cells is the basis of the AR-TIF2 PPIB assay. The assay was screened in two distinct formats, to identify small molecules that could block DHT-induced AR-TIF2 PPI formation or that could disrupt preexisting AR-TIF2 complexes. In addition to AR-TIF2 PPI inhibitors and disruptors, the AR-TIF2 PPIB assay also identifies AR antagonists and HSP 90 inhibitors.[27–29] **(B)** 10× Cropped gray-scale and color composite images representative of U-2 OS cells co-infected with the TIF2-GFP and AR-RFP recombinant adenoviruses, cultured overnight, and then treated ±25 nM DHT for 90 min were sequentially acquired on the IXM platform in three fluorescent channels; DAPI channel—Hoechst-stained nuclei that are *blue* in the color composite image; FITC channel—TIF2-GFP-positive nucleoli that are *green* in the color composite image; and Texas Red channel—AR-RFP, which is *red* in the color composite image. Exposure to AR agonists like DHT dramatically alters the AR-RFP subcellular distribution phenotype apparent in the Texas Red channel images and corroborated by the shift from *green* to *yellow* nucleoli in the composite images. Representative images from one of numerous separate experiments are presented. AR, androgen receptor; DHT, dihydrotestosterone; GFP, green fluorescent protein; HCS, high-content screening; HSP, heat shock protein; IXM, ImageXpress Micro; PPI, protein-protein interaction; PPIB, protein-protein interaction biosensor; RFP, red fluorescent protein; TIF2, transcriptional intermediary factor 2.

in nucleoli, as indicated in the cartoon and the bright yellow AR-TIF2 puncta within the blue Hoechst-stained nuclei of color composite images (*Fig. 1A, B*). Exposure to DHT dramatically alters the AR-RFP subcellular distribution phenotype in the Texas Red channel images and shifts the color of nucleoli in composite images from green to yellow (*Fig. 1B*).

We screened the AR-TIF2 PPIB assay in two distinct formats, typically processing 15 compound plates and 30×384-well assay plates per day of screening operations. To determine if compounds could block DHT-induced AR-TIF2 PPI formation, assay plates were preexposed to compounds for 3 h before treatment with 25 nM DHT for 90 min. To identify compounds that could disrupt preexisting AR-TIF2 PPI complexes, assay plates were preexposed to 25 nM DHT for 90 min before the transfer of compounds and an additional 3-h incubation. The MAIFI of AR-RFP within TIF2-GFP-positive nucleolar mask output of the TE image analysis module was used to quantify AR-TIF2 PPIs.[26–28] The MAIFI-AR-RFP data from maximum (DHT plus DMSO, $n=32$) and minimum (DMSO, $n=32$) plate control wells were used to define the assay signal window, calculate Z'-factor coefficients and S:B ratios, and to normalize the data from compound-treated wells (*Supplementary Fig. S1*; Supplementary Data are available online at www.liebertpub.com/adt). The AR-TIF2 PPIB assay performed robustly and reproducibly throughout the primary HCS campaign. In the format to find inhibitors of AR-TIF2 PPI formation, the mean Z'-factor coefficient was 0.71 ± 0.08 ($n=451$) and the mean S:B ratio was 7.8 ± 1.1 ($n=451$) (*Supplementary Fig. S1A, B*). Similarly, in the format to find disruptors of preexisting AT-TIF2 PPI complexes, the mean Z'-factor coefficient was 0.78 ± 0.07 ($n=451$) and the mean S:B ratio was 19.5 ± 3.3 ($n=451$) (*Supplementary Fig. S1C, D*). The larger average S:B ratio of the disruptor assay format reflects the longer DHT exposure period of 4.5 h versus 1.5 h in the inhibitor assay format. None of the assay plates in either assay format met our failed plate criteria of having both a Z'-factor coefficient ≤0.25 and an S:B ratio ≤3. However, 15 plates from the 83K NCI CBC library (plates 249–263) produced S:B ratios that were substantially lower than was typically observed throughout the HCS (*Supplementary Fig. S1C, D*), but since the corresponding Z'-factor coefficients for these plates were not ≤0.25, the plates passed our QC review criteria.

AR-TIF2 PPIB Primary HCS and Active Confirmation

We screened a total of 143,535 compounds from three compound libraries in the AR-TIF2 PPI HCS campaign (*Fig. 2* and *Table 1*). Compounds were screened at concentrations of 10 μg/mL, 25 μM, and 20 μM for the 10K ChemDiv PPI, 50K ChemBridge diversity, and 83K NCI CBC libraries, respectively. The % inhibition threshold for active compounds was set at ≥45% for the 10K ChemDiv library, and ≥40% for the other libraries (*Table 1*). In the primary HCS to find inhibitors of DHT-induced AR-TIF2 PPI formation, the median % inhibition was 11.5%, and 97.5% of the compounds were below our thresholds and scored inactive (*Fig. 2A* and *Table 1*). In the primary screen to identify disruptors of preexisting AR-TIF2 PPI complexes, the median % inhibition was 7.6%, and 99.3% of all compounds were below our thresholds and scored inactive (*Fig. 2B* and *Table 1*). We used a z-score plate-based statistical scoring method to flag compounds that behaved as outliers compared to the other substances ($n=320$, no controls) tested on an assay plate for selected HCS multiparameter measurement output by the image analysis module (*Table 1*).[31,33,42] We utilized the number of compartments that represents the number of TIF2-GFP-positive nucleoli identified in the FITC channel to flag compounds with z-scores <−3 as cytotoxic. We used z-scores for the mean average and integrated fluorescent intensity parameters from the DAPI, FITC, and Texas Red channels to flag compounds with z-scores >3 as fluorescent outliers. After applying the cytotoxic and fluorescent compound outlier analysis to the AR-TIF2 multiparameter HCS data, the number of qualified actives dropped to 1.93% and 0.57% for the AR-TIF2 inhibitor and disruptor screens, respectively (*Table 1*). All three of the compound libraries exhibited similar cytotoxic and fluorescent outlier rates, and essentially similar qualified active rates in the AR-TIF2 disruptor screen. In the AR-TIF2 inhibitor format, however, the qualified active rate for the three libraries was higher than in the disruptor format and differed among the libraries: 2.86%, 0.85%, and 1.95% for the 10K ChemDiv PPI, 50K ChemBridge diversity, and 83K NCI CBC libraries, respectively.

A total of 1,930 qualified active compounds were cherry picked and confirmed in triplicate wells at the original screening concentrations in both assay formats (*Fig. 3* and *Table 2*). The overall AR-TIF2 PPI active confirmation rate was relatively low at only 23% and 2.5% for the inhibitor and disruptor assay formats, respectively. Despite exhibiting the highest active rate in the primary HCS (*Table 1*), the 10K ChemDiv PPI library produced the lowest confirmation rate and fewest confirmed actives, including none in the disruptor format (*Fig. 3* and *Table 2*). The 50K ChemBridge and 83K NCI CBC libraries exhibited active confirmation rates of 21.5% and 30% in the AR-TIF2 inhibitor format, respectively, and 4.9% and 2.1% in the disruptor format (*Fig. 3* and *Table 2*).

Counter Screens

We used the p53-hDM2 PPIB HCS assay as a counter screen to determine whether active compounds interfered with the

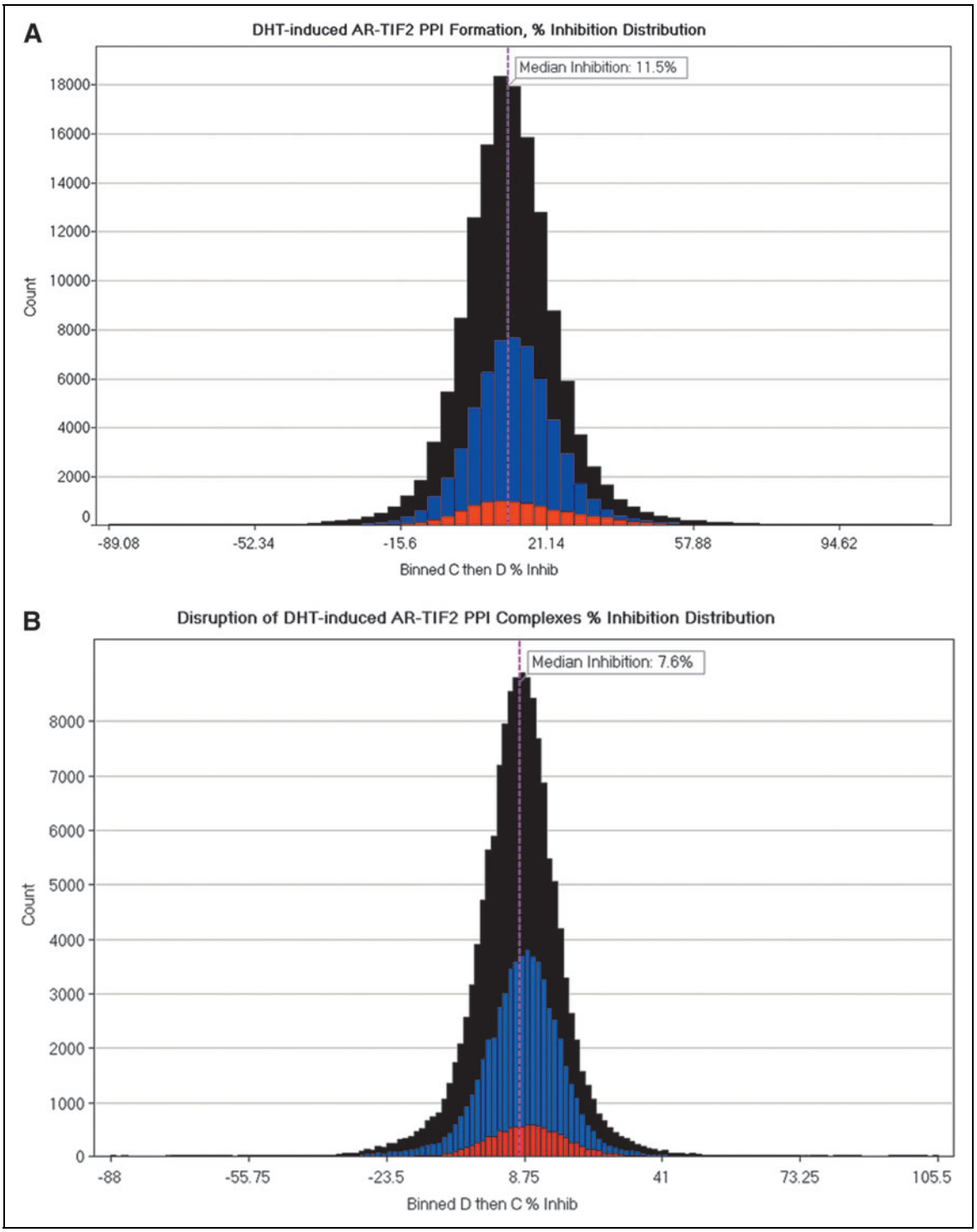

Fig. 2. Primary AR-TIF2 PPIB HCS campaign results summary; **(A)** inhibition of DHT-induced AR-TIF2 PPI formation and **(B)** disruption of preformed AR-TIF2 PPI complexes. Binned histograms of the normalized percent inhibition for the entire screening campaign to identify inhibitors of DHT-induced AR-TIF2 formation and disruptors of preexisting AR-TIF2 PPIs. Normalized % inhibition/disruption for each of the three compound libraries are indicated by color: (*red square*) 10K ChemDiv PPI library, (*blue square*) 50K ChemBridge diversity library, and (*black square*) 83K NCI CBC library.

Table 1. Androgen Receptor-Transcription Intermediary Factor 2 Protein-Protein Interaction Primary High-Content Screening Campaign Summary; Cytotoxic and Fluorescent Compound Outlier Analysis

	Inhibition of DHT-induced AR-TIF2 PPI formation[a]		Disruption of existing AR-TIF2 PPI complexes[b]	
	Compound then DHT		DHT then compound	
Compound library	Number	%	Number	%
10K[c] ChemDiv library @ 10 μg/mL				
Actives[d] that exhibited ≥45% inhibition	336	3.4	74	0.74
Inactives that exhibited <45% inhibition	9,664	96.6	9,926	99.3
Cytotoxic[e], compartment z-score <–3	53	0.53	75	0.75
FITC channel z-score >3	35	0.35	15	0.15
Texas Red channel z-score >3	47	0.47	19	0.19
Qualified[f] active	286	2.86	54	0.54
50K ChemBridge library @ 25 μM				
Actives that exhibited ≥40% inhibition	531	1.06	215	0.43
Inactives that exhibited <40% Inhibition	49,469	98.9	49,785	99.6
Cytotoxic, compartment z-score <–3	216	0.43	219	0.44
FITC channel z-score >3	59	0.12	31	0.06
Texas Red channel z-score >3	243	0.49	214	0.43
Qualified active	423	0.85	171	0.34
83K NCI library @ 20 μM				
Actives that exhibited ≥40% inhibition	2,699	3.23	686	0.82
Inactives that exhibited <40% inhibition	80,836	96.8	82,849	99.2
Cytotoxic, compartment z-score <–3	437	0.52	486	0.58
FITC channel z-score >3	965	1.16	953	1.14
Texas Red channel z-score >3	377	0.45	344	0.41
Qualified active	1,633	1.95	296	0.35
Primary HCS-qualified active sum	2,765	1.93	817	0.57

A total of 143,535 compounds from the three compound libraries were screened in singlicate wells at the indicated concentrations in the AR-TIF2 PPI HCS assay in two formats.

[a]To determine if compounds could block DHT-induced AR-TIF2 PPI formation, assay plates were preexposed to compounds for 3 h before treatment with 25 nM DHT for 90 min.

[b]To identify compounds that could disrupt preexisting AR-TIF2 PPI complexes, assay plates were preexposed to 25 nM DHT for 90 min before compound transfer and an additional 3-h incubation.

[c]K = 1,000 compounds.

[d]Compounds that met the activity threshold % inhibition criterion of ≥45% inhibition for the 10K ChemDiv library, or ≥40% inhibition for the 50K ChemBridge and 83K NCI libraries.

[e]A z-score plate-based statistical scoring method was used to flag compounds that behaved as outliers compared to the other substances ($n = 320$, no controls) tested on an assay plate. The number of compartments that represents the number of TIF2-GFP-positive nucleoli identified in the FITC channel was used to flag compounds with z-scores <–3 as cytotoxic. Compounds with z-scores >3 in one or more of the average or integrated fluorescent intensity parameters in any channel were flagged as fluorescent outliers.

[f]Qualified active compounds are those that met the appropriate activity threshold % inhibition criterion and were not flagged as either cytotoxic or fluorescent outliers.

AR, androgen receptor; DHT, dihydrotestosterone; GFP, green fluorescent protein; HCS, high-content screening; PPI, protein-protein interaction; TIF2, transcriptional intermediary factor 2.

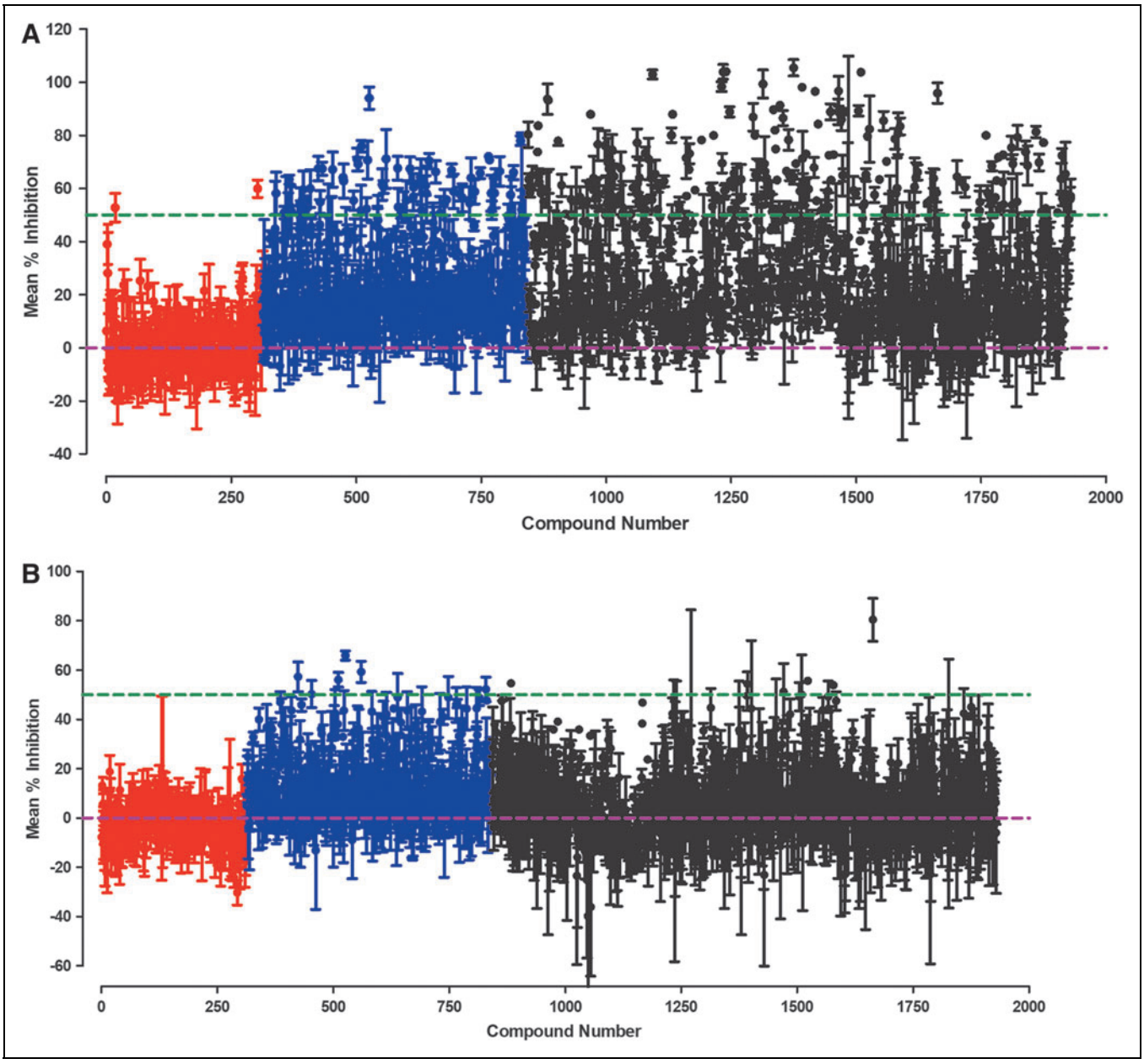

Fig. 3. Primary AR-TIF2 PPIB HCS active confirmation summary; **(A)** inhibition of DHT-induced AR-TIF2 PPI formation and **(B)** disruption of preformed AR-TIF2 PPI complexes. To confirm qualified actives flagged as inhibitors of AR-TIF2 formation or disruptors of preexisting AR-TIF2 complexes (>40% inhibition/disruption), we cherry picked and reformatted the compounds into 384-well active confirmation plates and rescreened them in triplicate wells in both primary assay formats. Normalized mean % inhibition/disruption ± SD ($n = 3$) for active compounds from each of the three compound libraries are indicated by color: (*red circle*) 10K ChemDiv PPI library, (*blue circle*) 50K ChemBridge diversity library, and (*black circle*) 83K NCI CBC library. The *dashed green line* indicates 50% inhibition/disruption threshold.

PPIB assay format or were nonspecific PPI disruptors.[30,31] Representative images of the p53-hDM2 PPI assay plate controls are presented in *Figure 4A*. After overnight culture of U-2 OS cells co-infected with the p53-GFP and hDM2-RFP adenovirus constructs, the hDM2-RFP shuttling partner co-localized with the p53-GFP partner anchored within the nucleoli of the Hoechst-stained nuclei, indicated by the similar punctate staining pattern of the two biosensors in the FITC and Texas Red channels, and the predominant yellow color of the nucleoli in the composite images of DMSO-treated cells (*Fig. 4A*). Exposure to the p53-hDM2 PPI disruptor Nutlin-3 at 10 μM for 30 min dramatically altered the hDM2-RFP

Table 2. Androgen Receptor-Transcription Intermediary Factor 2 Protein-Protein Interaction Active Confirmation Summary

	Inhibition of DHT-induced AR-TIF2 PPI formation[a]		Disruption of Existing AR-TIF2 PPI Complexes[b]	
	Compound then DHT		DHT then compound	
Compound library	Number	%	Number	%
10K[c] ChemDiv PPI library @ 10 μg/mL	314	100	314	100
Confirmed actives[d] mean inhibition ≥40% ($n=3$)	2	0.64	0	0
50K ChemBridge library @ 25 μM	530	100	530	100
Confirmed actives mean inhibition ≥40% ($n=3$)	114	21.5	26	4.91
83K NCI library @ 20 μM	1,086	100	1,086	100
Confirmed actives mean inhibition ≥40% ($n=3$)	327	30.1	23	2.12
Primary HCS qualified active sum	1,930	100	1,930	100
Confirmed actives mean inhibition >40% ($n=3$)	443	23.0	49	2.5

A total of 1,930 qualified active compounds from the primary HCS were cherry picked and confirmed in triplicate wells at the indicated concentrations in the AR-TIF2 PPI HCS assay in two formats.

[a]To determine if compounds could block DHT-induced AR-TIF2 PPI formation, assay plates were preexposed to compounds for 3 h before treatment with 25 nM DHT for 90 min.

[b]To identify compounds that could disrupt preexisting AR-TIF2 PPI complexes, assay plates were preexposed to 25 nM DHT for 90 min before compound transfer and an additional 3-h incubation.

[c]K = 1,000 compounds.

[d]Confirmed active compounds met the mean % inhibition threshold criterion of ≥40% ($n=3$).

subcellular distribution phenotype in the Texas Red channel images, where the hDM2-RFP shuttling partner redistributed into the cytoplasm, while the p53-GFP partner remained anchored within the nucleoli. This is indicated by the light green/blue nucleoli and predominantly red cytoplasm in the composite images (*Fig. 4A*). Exposure to the 427 confirmed AR-TIF2 PPI inhibitors or disruptors for 3 h had little or no effect on the hDM2-RFP subcellular distribution phenotype, indicating that none of the compounds disrupted p53-hDM2 PPIs or interfered with the biosensor assay format (*Fig 4B* and *Table 3*). In addition, only one of the confirmed AR-TIF2 PPI inhibitors or disruptors produced >50% cell loss under these conditions (*Fig. 4C*).

We used the Dex-induced GR-GFP nuclear translocation assay as a counter screen to identify compounds that potentially inhibited shared elements of nuclear receptor (NR) trafficking to the nucleus.[29,34] This assay also provided an NR

Fig. 4. p53-hDM2 PPI counter screen: **(A)** representative images of assay plate controls, and **(B)** % inhibition of p53-hDM2 PPIs and **(C)** % cell loss. **(A)** 10× Cropped gray-scale and color composite images for presentation purposes of U-2 OS cells co-infected with the p53-GFP and hDM2-RFP recombinant adenoviruses, cultured overnight, and then treated ±10 μM Nutlin-3 for 90 min were sequentially acquired on the IXM platform in three fluorescent channels: DAPI channel—Hoechst-stained nuclei that are *blue* in the color composite image; FITC channel—p53-GFP-positive nucleoli that are *green* in the color composite image; and Texas Red channel—hDM2-RFP, which is *red* in the color composite image. Exposure to p53-hDM2 PPI disruptors like Nutlin-3 dramatically alters the hDM2-RFP subcellular distribution phenotype apparent in the Texas Red channel images from the punctate nucleolar distribution colocalized within p53-GFP-positive nucleoli observed in untreated cells to a predominantly cytoplasmic hDM2-RFP distribution in Nutlin-3-treated cells. Nutlin-3 exposure induces a shift from *yellow* to *green* nucleoli in the composite images. Representative images from one of numerous separate experiments are presented. **(B)** Qualified actives that had been confirmed as AR-TIF2 PPI inhibitors or disruptors were cherry picked and tested in the p53-hDM2 PPIB counter screen assay to determine whether they also disrupted p53-hDM2 PPIs. The normalized % inhibition of p53-hDM2 PPIs is indicated on the *y*-axis and the activities of the compounds from the three compound libraries are depicted by the *closed symbols*: (*red closed circle*) 10K ChemDiv PPI library, (*blue closed circle*) 50K ChemBridge diversity library, and (*black closed circle*) 83K NCI CBC library. **(C)** The % of cell loss is indicated on the *y*-axis and the extent of cell loss by compounds from the three libraries are depicted by the *open symbols*: (*red open circle*) 10K ChemDiv PPI library, (*blue open circle*) 50K ChemBridge diversity library, and (*black open circle*) 83K NCI CBC library. The *dashed black line* represents the 50% threshold for p53-hDM2 PPI inhibition and cell loss, respectively, while the *dotted black line* represents the 0% threshold for both parameters.

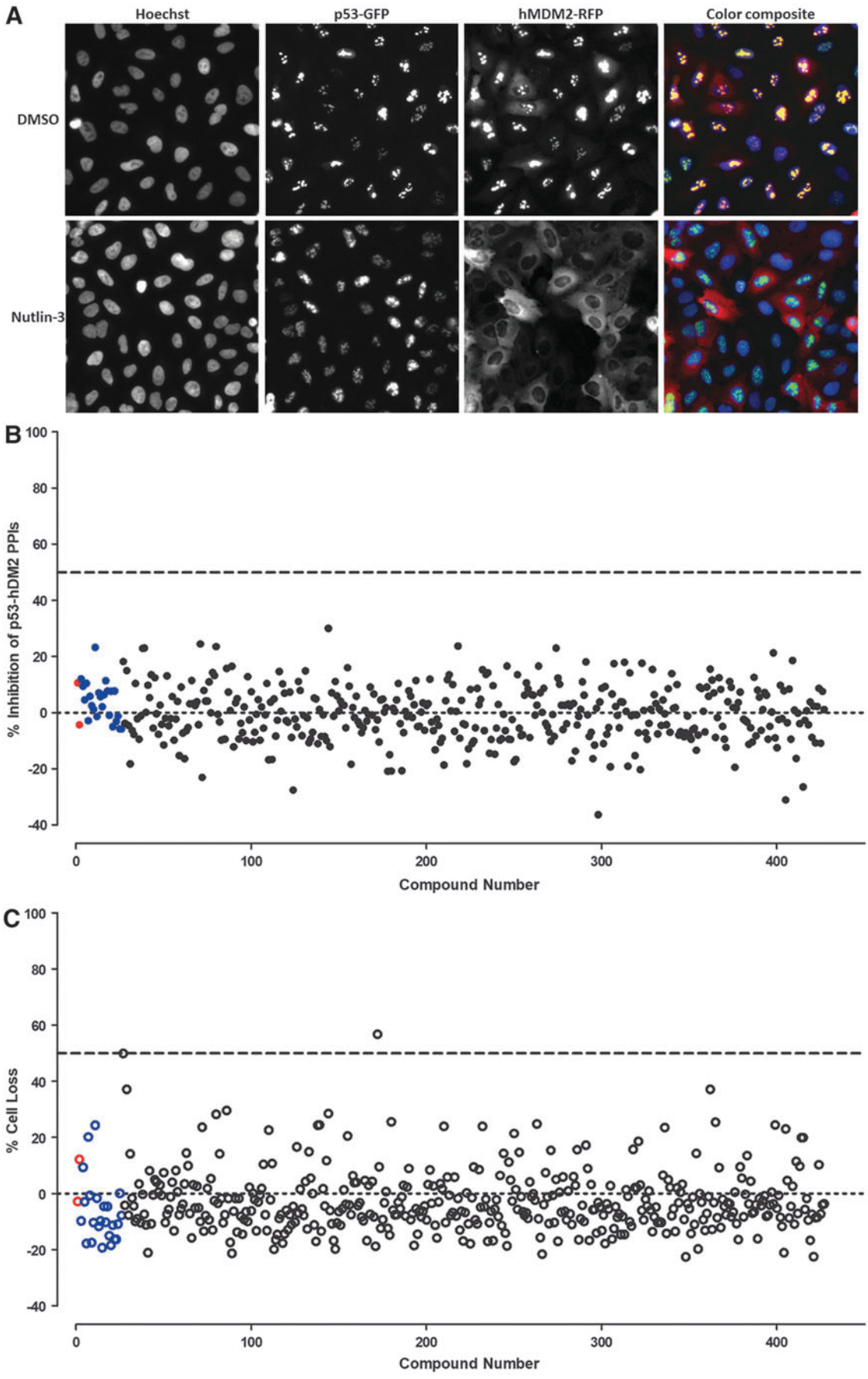

Table 3. Androgen Receptor-Transcription Intermediary Factor 2 Protein-Protein Interaction High-Content Screening Counter Screen Summary

	Counter screening assays					
	p53-hDM2 PPI[a]		GR-GFP NTL[b]		AR-GFP NL[c]	
Compound library	Number	%	Number	%	Number	%
10K[d] ChemDiv library @ 10 μg/mL	2	100	2	100	2	100
% Inhibition >50%	0	0	0	0	0	0
% Cell loss >50%	0	0	0	0	0	0
50K ChemBridge library @ 25 μM	24	100	24	100	24	100
% inhibition >50%	0	0	0	0	1	4.2
% Cell loss >50%	0	0	0	0	0	0
83K NCI library @ 20 μM	401	100	401	100	401	100
% Inhibition >50%	0	0	8	2.0	28	7.0
% Cell loss >50%	1	0.2	0	0	10	2.5
Confirmed qualified active	427	100	427	100	427	100
% Inhibition >50%	0	0	8	1.9	29	6.8
% Cell loss >50%	1	0.23	0	0.00	10	2.3

A total of 427 qualified active compounds that were confirmed in the AR-TIF2 PPI assay were cherry picked and tested in singlicate wells at the indicated concentrations in three counter screening assays.

[a]The p53-hDM2 PPI biosensor assay uses the same adenovirus chimeric biosensor co-infection assay format in U-2 OS cells as the AR-TIF2 assay, except that the protein-interacting partner components of the GFP and RFP fusion proteins are encoded by p53 and hDM2, respectively.

[b]The Dex-induced GR translocation counter screen provided a steroid nuclear receptor selectivity and/or specificity filter.

[c]The AR nuclear localization provided a way to identify compounds that altered AR-GFP subcellular localization independent of PPIs with a TIF2 biosensor.

[d]K = 1,000 compounds.

GR, glucocorticoid receptor; NL, nuclear localization; NTL, nuclear translocation; RFP, red fluorescent protein.

Fig. 5. Dexamethasone-induced GR-GFP nuclear translocation counter screen: **(A)** representative images of assay plate controls, and **(B)** % inhibition of Dex-induced GR-GFP nuclear translocation, and **(C)** % cell loss. **(A)** 10 × Cropped gray-scale and color composite images of Hoechst-stained nuclei and GR-GFP from 3617.4 cells that had been plated and cultured for 48 h under Tet-off conditions and were then treated with either 0.5% DMSO or 100 nM Dex and 0.5% DMSO for 30 min are presented. Images were sequentially acquired on the IXM platform in two fluorescent channels: DAPI channel—Hoechst-stained nuclei that are *blue* in the color composite image; and FITC channel—GR-GFP, which is *green* in the color composite image. Exposure to Dex alters the GR-GFP subcellular distribution phenotype apparent in the FITC channel and composite images from a predominantly cytoplasmic distribution in untreated 3617.4 cells to a predominantly nuclear distribution within the Hoechst-stained nuclei of Dex-treated cells. Representative images from one of numerous separate experiments are presented. **(B)** Qualified actives that had been confirmed as AR-TIF2 PPI inhibitors or disruptors were cherry picked and tested to determine whether they inhibited Dex-induced GR nuclear translocation. The normalized % inhibition of GR-GFP nuclear translocation is indicated on the *y*-axis and the activities of the compounds from the three libraries are depicted by the *closed symbols*: (*red closed circle*) 10K ChemDiv PPI library, (*blue closed circle*) 50K ChemBridge diversity library, and (*black closed circle*) 83K NCI CBC library. **(C)** The % of cell loss is indicated on the *y*-axis and the extent of cell loss produced by compounds from the three libraries are indicated by the *open symbols*: (*red open circle*) 10K ChemDiv PPI library, (*blue open circle*) 50K ChemBridge diversity library, and (*black open circle*) 83K NCI CBC library. The *dashed black line* represents the 50% threshold for p53-hDM2 PPI inhibition and cell loss, respectively, while the *dotted black line* represents the 0% threshold for both parameters. Dex, dexamethasone; DMSO, dimethyl sulfoxide; GR, glucocorticoid receptor; Tet, tetracycline.

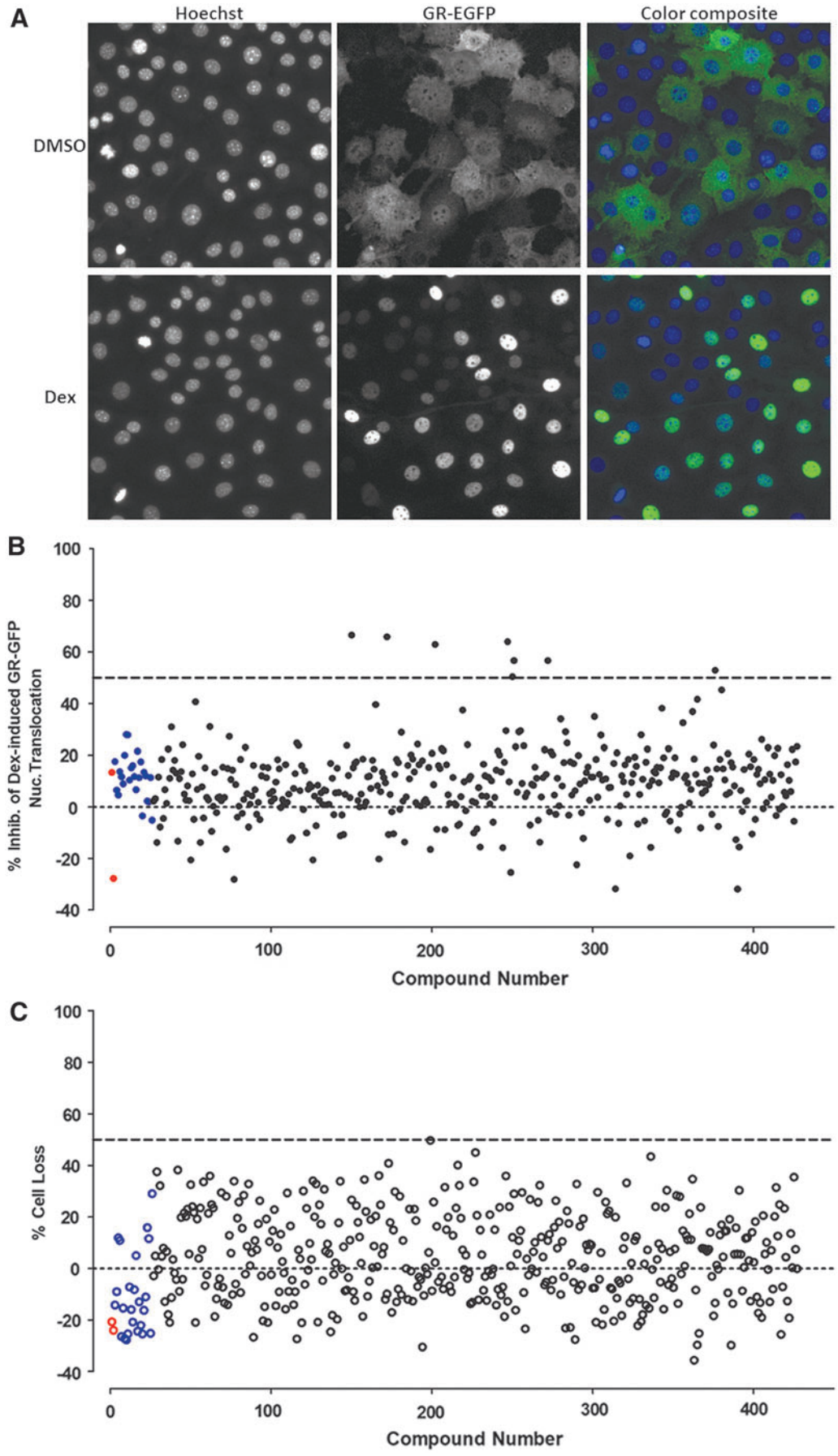

selectivity filter. Representative images of the GR-GFP nuclear translocation assay plate controls are presented in *Figure 5A*. Under Tet-off conditions, GR-GFP expression in 3617.4 cells was diffusely distributed throughout cells exposed to DMSO, although GR-GFP appeared to be more prominently localized in the cytoplasm compartment of a subpopulation of cells (*Fig. 5A*). In 3617.4 cells cultured under Tet-off conditions and exposed to 100 nM Dex for 30 min, however, the GR-GFP distribution phenotype was dramatically altered such that the GR-GFP was almost exclusively co-localized within Hoechst-stained nuclei (*Fig. 5A*). Eight of the confirmed active AR-TIF2 PPI inhibitors or disruptors also inhibited Dex-induced GR-GFP nuclear translocation when cells were preexposed to the compounds for 3 h before the addition of Dex (*Fig. 5B* and *Table 3*). Only one of the confirmed AR-TIF2 PPI inhibitors or disruptors produced close to 50% cell loss under these conditions (*Fig. 5C*).

The AR-GFP nuclear localization assay was used as a counter screen to identify compounds that reduced AR expression levels and/or shifted the predominant nuclear localization of AR into the cytoplasm.[33,43,44] Representative images of the AR-GFP nuclear localization assay plate controls are presented in *Figure 6A*. In N3 C4-2-2GFP-AR cells that were seeded into assay plates and cultured for 24 h before being exposed to DMSO overnight, the AR-GFP exhibits a predominantly nuclear distribution co-localized within Hoechst-stained nuclei (*Fig. 6A*). Overnight exposure to the HSP 90 inhibitor 17-AAG substantially alters the AR-GFP subcellular distribution phenotype apparent in the FITC channel and composite images to a predominantly cytoplasmic distribution (*Fig. 6A*). Overnight exposure to the majority of confirmed AR-TIF2 PPI inhibitors or disruptors inhibited the nuclear localization of AR-GFP somewhere in the range between 20% and 50%, although 29 (6.8%) of the compounds achieved >50% inhibition (*Fig. 6B* and *Table 3*). Under these overnight compound exposure conditions, 10 of the confirmed AR-TIF2 PPI inhibitors or disruptors produced >50% cell loss (*Fig. 6C*).

AR-TIF2 PPI Inhibitor and Disruptor IC_{50} Determinations

A total of 286 qualified confirmed active compounds were selected for testing in 10-point, twofold serial dilution AR-TIF2 PPI inhibitor and disruptor IC_{50} determinations starting at a maximum concentration of 40 μM (*Figs. 7* and *8* and *Table 4*). *Figure 7A* and *B* show representative quantitative MAIFI values of AR-RFP within TIF2-GFP-positive nucleoli for the maximum (DHT plus DMSO, $n=32$) and minimum (DMSO, $n=32$) plate control wells of the inhibitor and disruptor assay formats, respectively. The MAIFI-AR-RFP data from the plate controls were used to define the assay signal windows and to normalize the data from compound-treated wells. The normalized % inhibition of AR-TIF2 PPI curve fits for both the AR-TIF2 PPI inhibitor and disruptor assay formats of four selected hit compounds are presented in *Figure 7C–F*—PPS-000600232 (*Fig. 7C*), PPS-000600220 (*Fig. 7D*), PPS-000600231 (*Fig. 7E*), and PPS-000600229 (*Fig. 7F*). In the inhibition of DHT-induced AR-TIF2 PPI formation assay, the relative IC_{50}s for PPS-000600232, PPS-000600220, PPS-000600231, and PPS-000600229 were 8.85, 5.98, 9.35, and 9.49 μM, respectively, and in the disruption of preexisting AR-TIF2 complexes, their relative IC_{50}s were 6.72, 2.97, 5.56, and 12.62 μM, respectively. *Figures 8A* and *8B* show representative images of the AR-RFP subcellular distribution phenotypes for the DMSO and DHT plate controls and the 40 μM top concentrations of the same four hits in the AR-TIF2 PPI inhibitor and disruptor assay formats, respectively. *Supplementary Figure S2* shows the corresponding representative images of the TIF2-GFP subcellular distribution phenotypes

Fig. 6. AR-GFP nuclear localization counter screen: **(A)** representative images of assay plate controls, and **(B)** % inhibition of AR-GFP nuclear localization, and **(C)** % cell loss. **(A)** 10×Cropped gray-scale and color composite images of Hoechst-stained nuclei and AR-GFP from N3 C4-2-2GFP-AR cells that had been plated and cultured for 24 h and were then treated with either DMSO or DMSO plus 3.0 μM 17-AAG, and returned to the incubator and cultured overnight are presented. Images were sequentially acquired on the IXM platform in two fluorescent channels: DAPI channel—Hoechst-stained nuclei that are *blue* in the color composite image; and FITC channel—AR-GFP, which is *green* in the color composite image. Exposure to17-AAG alters the AR-GFP subcellular distribution phenotype apparent in the FITC channel and composite images from a predominantly nuclear distribution in untreated N3 C4-2-2GFP-AR cells to a predominantly cytoplasmic distribution in 17-AAG-treated cells. Representative images from one of numerous separate experiments are presented. **(B)** Qualified actives that had been confirmed as AR-TIF2 PPI inhibitors or disruptors were cherry picked and tested to determine whether they altered the nuclear localization of AR-GFP like 17-AAG. The normalized % inhibition of AR-GFP nuclear localization is indicated on the *y*-axis and the activities of the compounds from the three libraries are depicted by the *closed symbols*: (*red closed circle*) 10K ChemDiv PPI library, (*blue closed circle*) 50K ChemBridge diversity library, and (*black closed circle*) 83K NCI CBC library. **(C)** The % of cell loss is indicated on the *right y*-axis and the extent of cell loss produced by compounds from the three libraries is indicated by the *open symbols*: (*red open circle*) 10K ChemDiv PPI library, (*blue open circle*) 50K ChemBridge diversity library, and (*black open circle*) 83K NCI CBC library. The *dashed black line* represents the 50% threshold for AR-GFP nuclear localization and cell loss, respectively, while the *dotted black line* represents the 0% threshold for both parameters. 17-AAG, 17-allylaminogeldanamycin.

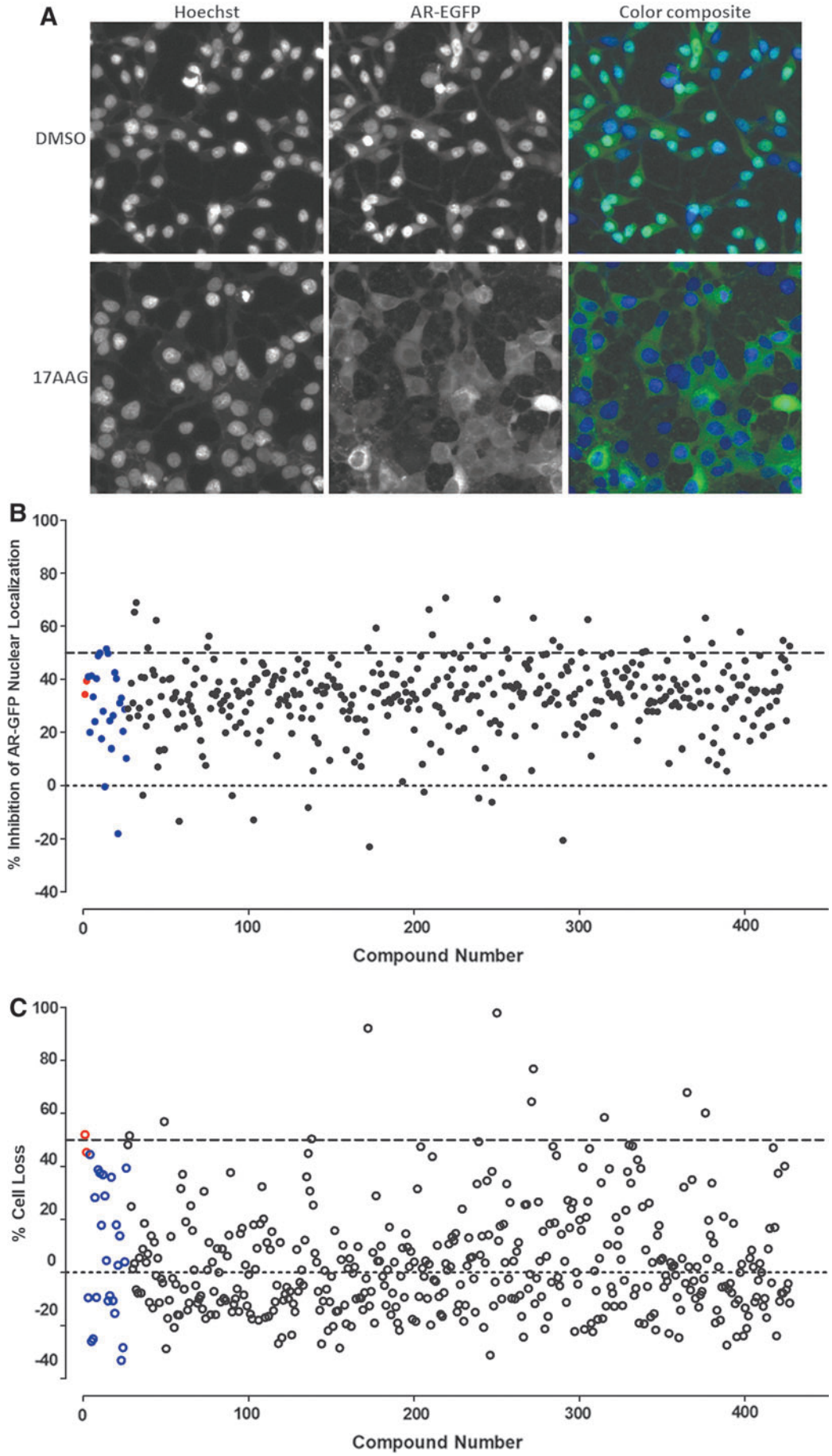

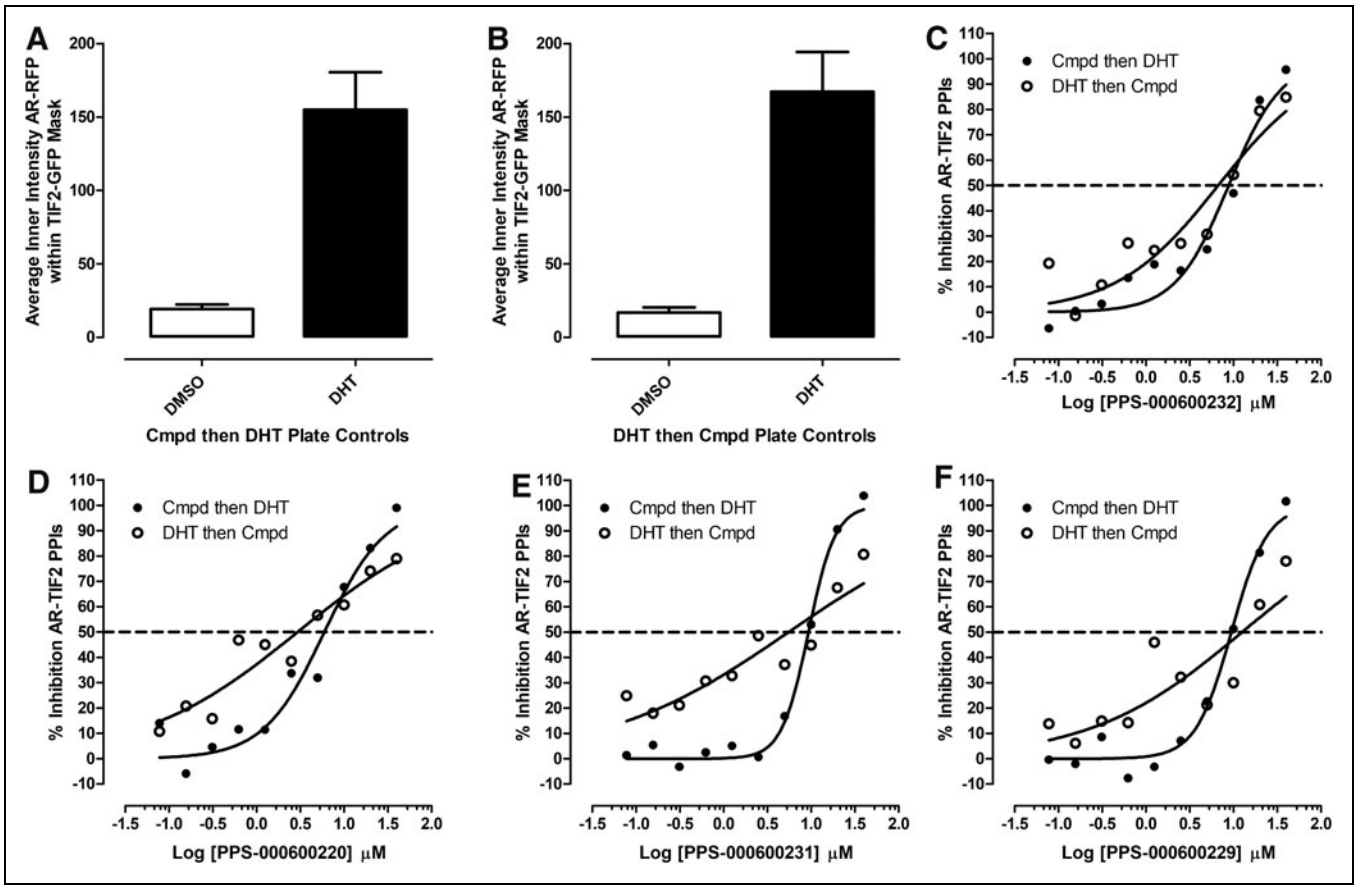

Fig. 7. AR-TIF2 PPI IC_{50} determinations: inhibition of DHT-induced AR-TIF2 PPI formation, and disruption of preformed AR-TIF2 PPI complexes. The mean average inner intensity of AR-RFP within the TIF2-GFP-positive nucleolus output of the TE image analysis module was used to quantify AR-TIF2 PPIs in the maximum (25 nM DHT+DMSO, $n=32$) and minimum (DMSO, $n=32$) plate control wells, and to normalize the data from compound-treated wells. The mean average AR-RFP inner intensity values ±SD ($n=32$) of control wells from plates that were treated with 25 nM DHT for 90 min either after or before 3-h exposure to hit compounds are presented in **(A)** and **(B)**, respectively. The normalized mean % inhibition of DHT-induced AR-TIF2 PPI formation and disruption of preformed AR-TIF2 PPI complexes at the indicated concentrations of selected hit compounds are shown; **(C)** PPS-000600232, **(D)** PPS-000600220 **(E)**, PPS-000600231, and **(F)** PPS-000600229. Representative IC_{50} curves from one of two independent 10-point, twofold serial dilution experiments conducted in singlicate wells and starting at a maximum concentration of 40 μM are presented. TE, translocation enhanced.

for the DMSO and DHT plate controls and the 40 μM top concentrations of the same four hits in the AR-TIF2 PPI inhibitor and disruptor assay formats. Importantly, none of the AR-TIF2 PPI inhibitor/disruptor hits altered the expression and/or nucleolar localization of the TIF2-GFP biosensor. Overall, 62.2% and 59.4% of the selected qualified confirmed actives produced reasonable quality curve fits with IC_{50}s < 40 μM in the inhibitor and disruptor assay formats, respectively (*Table 4*). The 10K ChemDiv PPI library produced the lowest IC_{50} confirmation rate, 35.7% and 7.1% in the inhibitor and disruptor format, respectively, and the fewest number of hits. The 83K NCI CBC library, which was the largest compound collection, produced an IC_{50} confirmation rate of 57.4% in both formats, and yielded 117 hits. The 50K ChemBridge diversity library had the highest IC_{50} confirmation rate, 82.4% and 76.5% in the inhibitor and disruptor format, respectively and yielded 52–56 hits.

DISCUSSION

We describe the successful implementation of the AR-TIF2 PPIB assay in an HCS campaign of 143,535 compounds from three distinct compound libraries (*Figs. 1* and *2*, *Supplementary Fig. S1*, and *Table 1*). The AR-TIF2 PPIB assay performed robustly and reproducibly throughout the primary HCS campaign, which enabled us to identify compounds that inhibited DHT-induced AR-TIF2 PPI formation and disrupted preexisting AR-TIF2 PPIs.

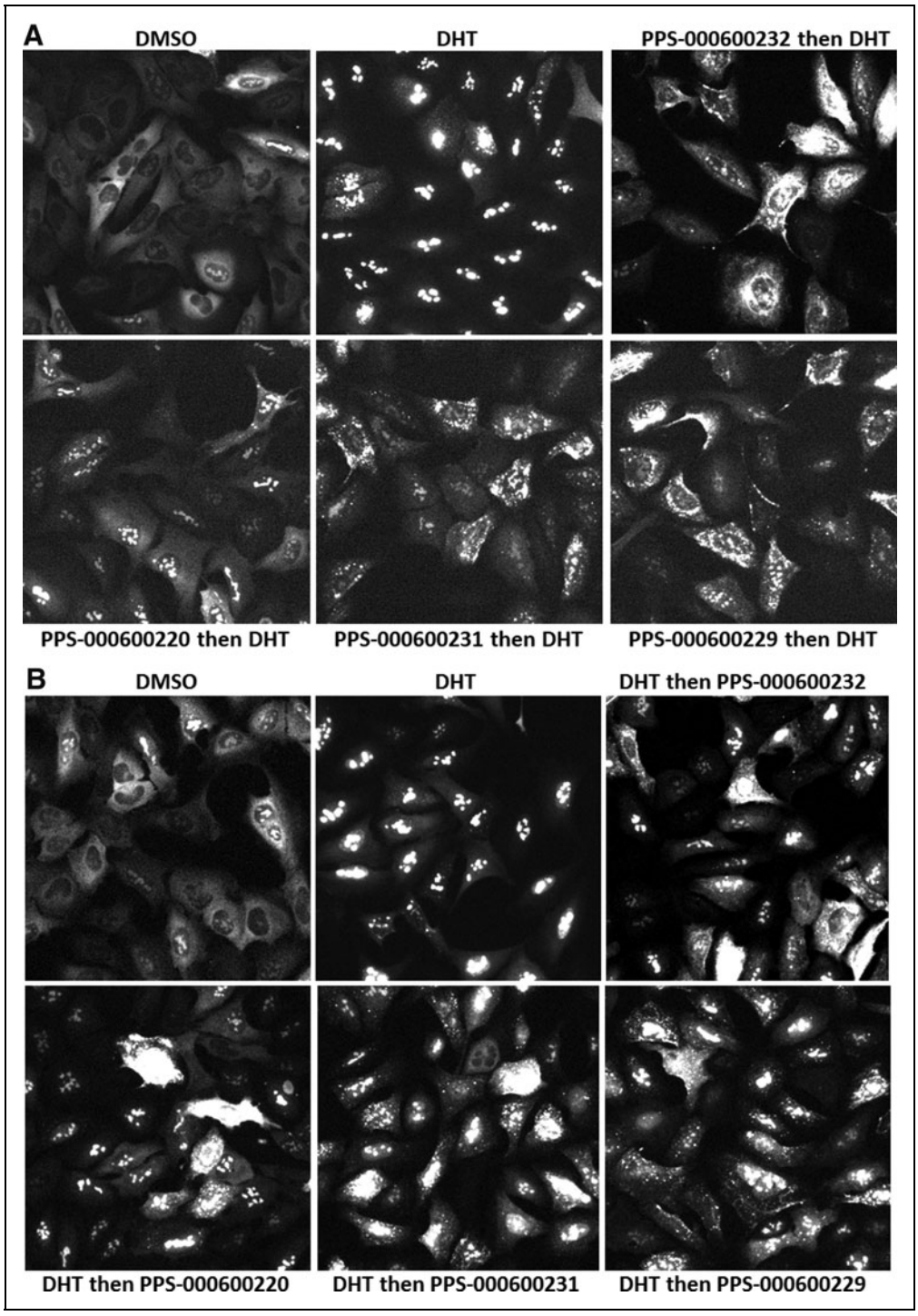

Fig. 8. Images of the AR-RFP distribution phenotypes of concentration-dependent AR-TIF2 PPI inhibitors and disruptors; **(A)** inhibition of DHT-induced AR-TIF2 PPI formation, and **(B)** disruption of preformed AR-TIF2 PPI complexes. 10× Cropped gray-scale images of the Texas Red channel AR-RFP subcellular distribution phenotypes in U-2 OS cells co-infected with the TIF2-GFP and AR-RFP biosensors, cultured overnight, and then treated with 25 nM DHT for 90 min either after **(A)** or before **(B)** 3-h exposure to selected hit compounds. Images from four distinct hit compound-treated wells that correspond to the quantitative data presented in *Figure 8* are shown. For comparison, images of the AR-RFP subcellular distribution phenotypes in DHT and DMSO control wells are also presented. Representative images from one of three independent experiments are presented.

HTS/HCS assay interference can be attributed to both chemical and physical compound properties.[39,45–51] For example, redox cycling compounds that generate hydrogen peroxide in cells or in biochemical HTS assay buffers containing strong reducing agents can indirectly inhibit the catalytic activity of protein tyrosine phosphatases, cysteine proteases, and metalloenzymes with active site residues susceptible to oxidation.[39,48,49,51–53] Compounds that are colored and fluorescent, or form aggregates have the potential to promiscuously interfere with a wide variety of biochemical and cell-based assay formats.[46,47,50,54,55] Using a strategy that we have used for other HCS campaigns, we applied a z-score plate-based statistical scoring method to the multiparameter HCS data to identify and deprioritize compounds that behaved as cytotoxic or autofluorescent outliers.[31,33,42] This allowed us to exclude 22.5% of the primary HCS active compounds before selecting qualified actives for confirmation (*Table 1*). The three compound libraries exhibited essentially similar cytotoxic and autofluorescent outlier rates, and similar qualified active rates in the AR-TIF2 PPI disruptor format. However, qualified active rates were higher in the AR-TIF2 PPI formation format and differed among libraries: 2.86% for the 10K ChemDiv PPI library, 0.85% for the 50K ChemBridge diversity library, and 1.95% for the 83K NCI CBC library.

Qualified active compounds were cherry picked and confirmed in triplicate wells at the original screening concentrations in both

Table 4. Androgen Receptor-Transcription Intermediary Factor 2 Protein-Protein Interaction IC_{50} Summary

	Inhibition of DHT-induced AR-TIF2 PPI formation[a]		Disruption of existing AR-TIF2 PPI complexes[b]	
	Compound then DHT		DHT then compound	
Compound library	Number	%	Number	%
10K[c] ChemDiv library @ 10 μg/mL	14	100	14	100
Hits that exhibited a calculable[d] IC_{50}	5	35.7	1	7.1
50K ChemBridge library @ 25 μM	68	100	68	100
Hits that exhibited a calculable IC_{50}	56	82.4	52	76.5
83K NCI library @ 20 μM	204	100	204	100
Hits that exhibited a calculable IC_{50}	117	57.4	117	57.4
AR-TIF2-qualified confirmed actives sum	286	100	286	100
Hits that exhibited a calculable IC_{50}	178	62.2	170	59.4
AR-TIF2 IC_{50} range μM				
<1 μM	0	0	2	1.2
1–10 μM	32	18.0	68	40.0
10–40 μM	146	82.0	100	58.8

A total of 286 qualified confirmed active compounds from the three libraries were tested in two independent 10-point, twofold serial dilution experiments conducted in singlicate wells and starting at a maximum concentration of 40 μM in the AR-TIF2 PPI HCS assay performed in two formats.

[a]To determine if compounds could block DHT-induced AR-TIF2 PPI formation, assay plates were preexposed to compounds for 3 h before treatment with 25 nM DHT for 90 min.

[b]To identify compounds that could disrupt preexisting AR-TIF2 PPI complexes, assay plates were preexposed to 25 nM DHT for 90 min before compound transfer and an additional 3-h incubation.

[c]K = 1,000 compounds.

[d]Compounds that produced curve fits with IC_{50}s < 40 μM.

IC_{50}, 50% inhibition concentration.

AR-TIF2 PPIB assay formats (*Fig. 3* and *Table 2*). The relatively low qualified active confirmation rates of 23% and 2.5% for the AR-TIF2 inhibitor and disruptor formats, respectively, were the result of two strategic decisions. First, because we decided to cast a wide net by setting a low % inhibition threshold as our active criterion, ≥40–45% depending upon the library, many of the AR-TIF2 primary HCS actives close to the threshold failed to confirm (*Fig. 3* and *Table 2*). Second, the 10-fold lower confirmation rate observed in the AR-TIF2 PPI disruptor format was because we confirmed qualified actives in both AR-TIF2 assay formats, irrespective of their activity in these formats in the primary screen.

The p53-hDM2 PPIB counter screen uses the same adenovirus chimeric biosensor co-infection assay format and PPI detection strategy in U-2 OS cells as the AR-TIF2 assay, except that the protein-interacting partner components of the chimeric GFP and RFP fusion protein biosensors contain the interacting domains from p53 and hDM2, respectively.[30–32] The p53-hDM2 PPIB assay therefore serves as both an assay format interference and PPI selectivity counter screen.[26] None of the fifteen AR-TIF2 PPIB hits from the Library of Pharmacologically Active Compounds (LOPAC) set interfered with the biosensor assay format or inhibited p53-hDM2 PPIs.[26] Similarly, none of the confirmed AR-TIF2 PPI inhibitors or disruptors from the current HCS campaign altered the hDM2-RFP subcellular distribution phenotype (*Fig 4B* and *Table 3*), indicating that they are unlikely to be either nonselective PPI inhibitors or to interfere with the biosensor assay format.

Both AR and GR are members of the steroid receptor subfamily of NRs.[29,34] Like AR, the folding of *de novo* synthesized GR and its maturation to a conformational state capable of high-affinity hormone binding occurs in the cytoplasm and

involves contributions from molecular chaperones and co-chaperones.[29,34] Ligand binding induces GR trafficking from the cytoplasm to the nucleus, entry through the nuclear pore complex, binding to specific glucocorticoid response element DNA sequences in the promoter/enhancer regions of target genes, and modulation of gene transcription levels.[29,34] The Dex-induced GR-GFP nuclear translocation assay provides a steroid NR selectivity counter screen that also shares components of the AR signaling pathway. Components shared by the AR and GR signaling pathways include the HSP 90 and HSP 70 chaperones that maintain both NRs in high-affinity structural conformations for ligand binding, ligand-bound AR and GR that are both cargos of dynein-mediated retrograde trafficking along microtubules to the nucleus, and the importin-α/β adaptor system that mediates entry through the nuclear pore complex for both NRs.[21,22,29,34,56–58] In the LOPAC screen, none of the steroidal AR-TIF2 PPIB hits inhibited Dex-induced GR-GFP nuclear translocation, but all five of the nonsteroidal hits did.[26,29,34] Confirmed actives in the AR-TIF2 PPIB assay that also inhibit GR nuclear translocation either lack AR specificity/selectivity or they inhibit a shared component of the AR and GR signaling pathways. We therefore deprioritized the eight confirmed AR-TIF2 PPIB actives that also inhibited GR-GFP nuclear translocation by >50% (*Fig. 5B* and *Table 3*).

Previously, we have used the AR-GFP nuclear localization assay to identify compounds that reduced AR expression levels and/or shifted the predominant nuclear localization of AR in CRPC cells into the cytoplasm.[33,43,44] The AR-TIF2 PPIB hits from the LOPAC set either enhanced AR-GFP nuclear localization or were inactive, suggesting that some hits were partial AR agonists and therefore would not be expected to inhibit or disrupt AR-TIF2 PPIs.[26] Compounds that could reduce AR-RFP biosensor expression levels or restrict its localization to the cytoplasm would be expected to inhibit the AR-TIF2 PPIB assay. Similarly, compounds that inhibit AR-RFP trafficking and nuclear entry, or that promote its nuclear export, might also be expected to inhibit the AR-TIF2 PPIB assay. Known AR antagonists such as flutamide and bicalutamide, and the HSP 90 inhibitor 17-AAG, inhibit the AR-TIF2 PPIB assay and produce a predominantly cytoplasmic AR-RFP distribution phenotype.[26–28] AR antagonists block DHT binding to the AR-RFP biosensor, and HSP 90 inhibitors prevent the molecular chaperone-mediated maturation of the AR-RFP biosensor into a conformational state capable of high-affinity ligand binding. AR antagonists and HSP 90 inhibitors block DHT-induced translocation of the AR-RFP biosensor into the nucleus, thereby preventing the PPIs with the TIF2-GFP biosensor anchored in the nucleolus that results in the accumulation and colocalization of AR-RFP in TIF2-GFP-positive nucleoli.[26–28] Twenty-nine (6.8%) of the confirmed AR-TIF2 PPI inhibitors/disruptors also reduced AR-GFP nuclear localization by >50% (*Fig. 6B* and *Table 3*), suggesting that they might be indirectly inhibiting the AR-TIF2 PPIB assay rather than directly blocking/disrupting PPIs.

A total of 62.2% of the qualified confirmed actives inhibited DHT-induced AR-TIF2 PPI formation in a concentration-dependent manner with IC_{50}s < 40 μM, and 59.4% also disrupted preexisting AR-TIF2 PPI complexes in a concentration-dependent manner (*Figs. 7* and *8* and *Table 4*). Critically, none of the AR-TIF2 PPI inhibitor/disruptor hits altered the expression and/or nucleolar localization of the TIF2-GFP biosensor (*Supplementary Fig. S2*). The IC_{50}s are in the range that one would reasonably anticipate for PPI inhibitors and disruptors from a high-throughput screen. Although most of the hits were active in both AR-TIF2 PPIB assay formats and altered the AR-RFP distribution phenotype similarly (*Fig. 8*), the IC_{50} values for the inhibition of AR-TIF2 PPI formation were typically lower and exhibited complete response curves with two asymptotes and r^2 values >0.95 (*Fig. 7C–F*). In the disruption of preexisting AR-TIF2 PPI format, the IC_{50} data typically exhibited response curves with maximal inhibition levels around 80%, and r^2 values in the 0.7 to 0.9 range (*Fig. 7C–F*). The overall hit rate for the 143,535-compound AR-TIF2 PPIB HCS campaign was 0.12% in both assay formats. The 10K ChemDiv PPI library was the smallest compound collection screened and despite having the highest primary HCS active rate, it exhibited the lowest hit rate of 0.05%. The 50K ChemBridge diversity library and the 83K NCI CBC library had hit rates of 0.11% and 0.14%, respectively.

We have begun to characterize and triage the hits from the AR-TIF2 PPIB HCS campaign in a panel of established secondary and tertiary assays (article in preparation).[26] We used competitive displacement binding assays between H^3-DHT and purified recombinant His_6-AR-LBD to identify and deprioritize hits that are AR antagonists. We used a PSA promoter-driven luciferase reporter assay performed in C4-2 CRPC cells to confirm that the AR-TIF2 PPI hits inhibited AR-mediated transcriptional activity. We have also developed mammalian 2-hybrid reporter assays that measure co-activator PPIs between AR-LBD-GAL4 and either TIF2-VP16 or SRC-1-VP16. The mammalian 2-hybrid assays were used to confirm that hits inhibit and/or disrupt AR co-activator PPIs, and to evaluate whether they were selective for AR interactions with TIF2 versus SRC-1. We hypothesized that AR-TIF2 PPI hits should be more effective at inhibiting the growth of PCa cell lines that express AR over those that do not. To test this, we implemented growth inhibition assays in LnCaP, C4-2, and 22-Rv1 cells, which express AR and TIF2, versus PC-3 and DU-145 that express TIF2, but not AR. We anticipate that this

testing paradigm will allow us to select AR-TIF2 PPI inhibitor/disruptor hits that are suitable starting points for medicinal chemistry lead optimization and might ultimately be developed into novel therapeutics for PCa and CRPC.

ACKNOWLEDGMENTS

The studies reported herein were funded by grant support from the National Institutes of Health (NIH); R21NS073889 Johnston (PI) from the NINDS; and R01CA160423 and R01CA183882 Johnston (PI) from the NCI.

DISCLOSURE STATEMENT

No competing financial interests exist.

REFERENCES

1. Siegel R, Naishadham D, Jemal A: Cancer statistics, 2013. *CA Cancer J Clin* 2013;63:11–30.
2. Kirby M, Hirst C, Crawford ED: Characterising the castration-resistant prostate cancer population: a systematic review. *Int J Clin Pract* 2011;65:1180–1192.
3. Keyes M, Crook J, Morton G, Vigneault E, Usmani N, Morris WJ: Treatment options for localized prostate cancer. *Can Fam Physician* 2013;59:1269–1274.
4. Gudziak MR, Smith AY: Hormonal therapy for stage D cancer of the prostate. *West J Med* 1994;160:351–359.
5. Harris WP, Mostaghel EA, Nelson PS, Montgomery B: Androgen deprivation therapy: progress in understanding mechanisms of resistance and optimizing androgen depletion (vol 6, pg 76, 2009). *Nat Clin Pract Urol* 2009;6:173–173.
6. Scher HI, Fizazi K, Saad F, *et al.*: Increased survival with enzalutamide in prostate cancer after chemotherapy. *N Engl J Med* 2012;367:1187–1197.
7. de Bono JS, Logothetis CJ, Molina A, *et al.*: Abiraterone and increased survival in metastatic prostate cancer. *N Engl J Med* 2011;364:1995–2005.
8. Karantanos T, Corn PG, Thompson TC: Prostate cancer progression after androgen deprivation therapy: mechanisms of castrate resistance and novel therapeutic approaches. *Oncogene* 2013;32:5501–5511.
9. Gregory CW, He B, Johnson RT, *et al.*: A mechanism for androgen receptor-mediated prostate cancer recurrence after androgen deprivation therapy. *Cancer Res* 2001;61:4315–4319.
10. Grossmann ME, Huang H, Tindall DJ: Androgen receptor signaling in androgen-refractory prostate cancer. *J Natl Cancer Inst* 2001;93:1687–1697.
11. Dehm SM, Tindall DJ: Molecular regulation of androgen action in prostate cancer. *J Cell Biochem* 2006;99:333–344.
12. Agoulnik I, Vaid, A, Nakka, M, *et al.*: Androgens modulate expression of transcription intermediary factor 2, an androgen receptor coactivator whose expression level correlates with early biochemical recurrence in prostate cancer. *Cancer Res* 2006;66:10594–10602.
13. Culig Z, Santer FR: Androgen receptor co-activators in the regulation of cellular events in prostate cancer. *World J Urol* 2012;30:297–302.
14. Culig Z, Santer FR: Molecular aspects of androgenic signaling and possible targets for therapeutic intervention in prostate cancer. *Steroids* 2013;78:851–859.
15. Fujimoto N, Miyamoto H, Mizokami A, *et al.*: Prostate cancer cells increase androgen sensitivity by increase in nuclear androgen receptor and androgen receptor coactivators; a possible mechanism of hormone-resistance of prostate cancer cells. *Cancer Invest* 2007;25:32–37.
16. Godoy A, Sotomayor PC, Villagran M, *et al.*: Altered corepressor SMRT expression and recruitment to target genes as a mechanism that change the response to androgens in prostate cancer progression. *Biochem Biophys Res Commun* 2012;423:564–570.
17. Gregory C, Johnson RT Jr, Mohler JL, French FS, Wilson EM: Androgen receptor stabilization in recurrent prostate cancer is associated with hypersensitivity to low androgen. *Cancer Res* 2001;61:2892–2898.
18. Koehler A. A complex task? Direct modulation of transcription factors with small molecules. *Curr Opin Chem Biol* 2010;14:331–340.
19. Schulman I, Heyman RA. The flip side: identifying small molecule regulators of nuclear receptors. *Chem Biol* 2004;11:639–646.
20. Shi X, Xue L, Zou JX, Gandour-Edwards R, Chen H, deVere White RW: Prolonged androgen receptor loading onto chromatin and the efficient recruitment of p160 coactivators contribute to androgen-independent growth of prostate cancer cells. *Prostate* 2008;68:1816–1826.
21. Culig Z, Hobisch A, Bartsch G, Klocker H: Androgen receptor—an update of mechanisms of action in prostate cancer. *Urol Res* 2000;28:211–219.
22. Culig Z, Klocker H, Bartsch G, Hobisch A: Androgen receptors in prostate cancer. *Endocr Relat Cancer* 2002;9:155–170.
23. Linja M, Porkka KP, Kang Z, *et al.*: Expression of androgen receptor coregulators in prostate cancer. *Clin Cancer Res* 2004;10:1032–1040.
24. Berrevoets CA, Doesburg P, Steketee K, Trapman J, Brinkmann AO: Functional interactions of the AF-2 activation domain core region of the human androgen receptor with the amino-terminal domain and with the transcriptional coactivator TIF2 (transcriptional intermediary factor2). *Mol Endocrinol* 1998;12:1172–1183.
25. Feng S, Tang Q, Sun M, Chun JY, Evans CP, Gao AC: Interleukin-6 increases prostate cancer cells resistance to bicalutamide via TIF2. *Mol Cancer Ther* 2009;8:665–671.
26. Fancher A, Hua Y, Camarco DP, Close DA, Strock CJ, Johnston PA. Reconfiguring the AR-TIF2 protein-protein interaction HCS assay in prostate cancer cells and characterizing the hits from a LOPAC screen. *Assay Drug Dev Technol* 2016;14:453–477.
27. Hua Y, Shun TY, Strock CJ, Johnston PA: High-content positional biosensor screening assay for compounds to prevent or disrupt androgen receptor and transcriptional intermediary factor 2 protein-protein interactions. *Assay Drug Dev Technol* 2014;12:395–418.
28. Hua Y, Camarco DP, Strock CJ, Johnston PA: High content positional biosensor assay to screen for compounds that prevent or disrupt androgen receptor and transcription intermediary factor 2 protein-protein interactions. *Methods Mol Biol* 2018;1683:211–227.
29. Daghestani H, Zhu G, Johnston PA, Shinde SN, Brodsky JL, Day BW: Characterization of inhibitors of glucocorticoid receptor nuclear translocation: a model of cytoplasmic dynein-mediated cargo transport. *Assay Drug Dev Technol* 2011;9:46–60.
30. Dudgeon D, Shinde SN, Shun TY, *et al.*: Characterization and optimization of a novel protein-protein interaction biosensor HCS assay to identify disruptors of the interactions between p53 and hDM2. *Assay Drug Dev Technol* 2010;8:437–458.
31. Dudgeon D, Shinde SN, Hua Y, *et al.*: Implementation of a 220,000 compound HCS campaign to identify disruptors of the interaction between p53 and hDM2, and characterization of the confirmed hits. *J Biomol Screen* 2010;15:152–174.
32. Hua Y, Strock CJ, Johnston PA: High content screening biosensor assay to identify disruptors of p53-hDM2 protein-protein interactions. *Methods Mol Biol* 2015;1278:555–565.
33. Johnston P, Nguyen MM, Dar JA, *et al.*: Development and implementation of a high-throughput high-content screening assay to identify inhibitors of androgen receptor nuclear localization in castration-resistant prostate cancer cells. *Assay Drug Dev Technol* 2016;14:226–239.
34. Johnston PA, Shinde SN, Hua Y, Shun TY, Lazo JS, Day BW: Development and validation of a high-content screening assay to identify inhibitors of cytoplasmic dynein-mediated transport of glucocorticoid receptor to the nucleus. *Assay Drug Dev Technol* 2012;10:432–456.
35. Htun H, Barsony J, Renyi I, Gould DL, Hager GL: Visualization of glucocorticoid receptor translocation and intranuclear organization in living cells with a green fluorescent protein chimera. *Proc Natl Acad Sci U S A* 1996;93:4845–4850.

36. McNally J, Müller WG, Walker D, Wolford R, Hager GL: The glucocorticoid receptor: rapid exchange with regulatory sites in living cells. *Science* 2000;287: 1262–1265.
37. Walker D, Htun H, Hager GL. Using inducible vectors to study intracellular trafficking of GFP-tagged steroid/nuclear receptors in living cells. *Methods* 1999;19:386–393.
38. Johnston P, Foster CA, Shun TY, et al. Development and implementation of a 384-well homogeneous fluorescence intensity high-throughput screening assay to identify mitogen-activated protein kinase phosphatase-1 dual-specificity protein phosphatase inhibitors. *Assay Drug Dev Technol* 2007;5: 319–332.
39. Johnston P, Soares KM, Shinde SN, et al. Development of a 384-well colorimetric assay to quantify hydrogen peroxide generated by the redox cycling of compounds in the presence of reducing agents. *Assay Drug Dev Technol* 2008;6:505–518.
40. Johnston P, Foster CA, Tierno MB, et al. Characterization of the Cdc25B dual specificity phosphatase inhibitor hits identified in a high throughput screen of the NIH compound library. *Assays Drug Dev Technol* 2009;7:250–265.
41. Johnston P, Sen M, Hua Y, *et al.*: High-content pSTAT3/1 imaging assays to screen for selective inhibitors of STAT3 pathway activation in head and neck cancer cell lines. *Assay Drug Dev Technol* 2014;12:55–79.
42. Johnston P, Sen M, Hua Y, *et al.*: HCS campaign to identify selective inhibitors of IL-6-induced STAT3 pathway activation in head and neck cancer cell lines. *Assay Drug Dev Technol* 2015;13:356–376.
43. Masoodi K, Xu Y, Dar JA, *et al.*: Inhibition of androgen receptor nuclear localization and castration-resistant prostate tumor growth by pyrroloimidazole-based small molecules. *Mol Cancer Ther* 2017;16:2120–2129.
44. Masoodi K, Eisermann K, Yang Z, *et al.*: Inhibition of androgen receptor function and level in castration-resistant prostate cancer cells by 2-[(isoxazol-4-ylmethyl)thio]-1-(4-phenylpiperazin-1-yl)ethanone. *Endocrinology* 2017; 158:3152–3161.
45. Auld DS, Southall NT, Ajit Jadhav, *et al.*: Characterization of chemical libraries for luciferase inhibitory activity. *J Med Chem* 2008;51:2372–2386.
46. Baell J, Holloway GA: New substructure filters for removal of pan assay interference compounds (PAINS) from screening libraries and for their exclusion in bioassays. *J Med Chem* 2010;53:2719–2740.
47. Inglese J, Johnson RL, Simeonov A, *et al.*: High-throughput screening assays for the identification of chemical probes. *Nat Chem Biol* 2007;3:466–479.
48. Lor L, Schneck J, McNulty DE, *et al.*: A simple assay for detection of small-molecule redox activity. *J Biomol Screen* 2007;12:881–890.
49. Soares K, Blackmon N, Shun TY, *et al.*: Profiling the NIH small molecule repository for compounds that generate H(2)O(2) by redox cycling in reducing environments. *Assay Drug Dev Technol* 2010;8:152–174.
50. Thorne N, Auld DS, Inglese J: Apparent activity in high-throughput screening: origins of compound-dependent assay interference. *Curr Opin Chem Biol* 2010; 14:315–324.
51. Johnston P: Redox cycling compounds generate H2O2 in HTS buffers containing strong reducing reagents—real hits or promiscuous artifacts? *Curr Opin Chem Biol* 2011;15:174–182.
52. Bova MP, Mattson MN, Vasile S, *et al.*: The oxidative mechanism of action of ortho-quinone inhibitors of protein-tyrosine phosphatase [alpha] is mediated by hydrogen peroxide. *Arch Biochem Biophys* 2004;429:30–41.
53. Smith GK, Barrett DG, Blackburn K, *et al.*: Expression, preparation, and high-throughput screening of caspase-8: discovery of redox-based and steroid diacid inhibition. *Arch Biochem Biophys* 2002;399:195–205.
54. Johnston PA, Johnston PA: Cellular platforms for HTS: three case studies. *Drug Discov Today* 2002;7:353–363.
55. Simeonov A, Jadhav A, Thomas C, *et al.*: Fluorescence spectroscopic profiling of compound libraries. *J Med Chem* 2008;51.
56. Burd C, Morey LM, Knudsen KE: Androgen receptor corepressors and prostate cancer. *Endocr Relat Cancer* 2006;13:979–994.
57. Chmelar R, Buchanan G, Need EM, Tilley W, Greenberg NM: Androgen receptor coregulators and their involvement in the development and progression of prostate cancer. *Int J Cancer* 2006;120:719–733.
58. Saporita A, Ai J, Wang Z: The Hsp90 inhibitor, 17-AAG, prevents the ligand-independent nuclear localization of androgen receptor in refractory prostate cancer cells. *Prostate* 2007;67:509–520.

Address correspondence to:
Paul A. Johnston, PhD
Department of Pharmaceutical Sciences
School of Pharmacy, Room 4101
Pittsburgh Tecnology Center
700 Technology Drive
Pittsburgh, PA 15219

E-mail: paj18@pitt.edu

Abbreviations Used

17-AAG = 17-allylaminogeldanamycin
ADT = androgen deprivation therapy
AF2 = activation function 2
AR = androgen receptor
AREs = androgen-responsive elements
AR-LBD = androgen receptor ligand binding domain
CRPC = castration-resistant prostate cancer
Dex = dexamethasone
DHT = dihydrotestosterone
DMEM = Dulbecco's modified Eagle's medium
DMSO = dimethyl sulfoxide
FBS = fetal bovine serum
GFP = green fluorescent protein
GR = glucocorticoid receptor
HCS = high-content screening
HSP = heat shock protein
IXM = ImageXpress Micro
LOPAC = Library of Pharmacologically Active Compounds
MAIFI = mean average inner fluorescent intensity
NLS = nuclear localization sequence
NES = nuclear export sequence
NoLS = nucleolar localization sequence
NR = nuclear receptor
PBS = phosphate-buffered saline
PCa = prostate cancer
PPI = protein-protein interaction
PPIB = protein-protein interaction biosensor
PSA = prostate specific antigen
QC = quality control
RFP = red fluorescent protein
S:B = signal-to-background ratio
TE = translocation enhanced
Tet = tetracycline
TIF2 = transcriptional intermediary factor 2